Electrical Stimulation of Mammalian Retinal Ganglion Cells With Multielectrode Arrays

Chris Sekirnjak, Pawel Hottowy, Alexander Sher, Wladyslaw Dabrowski, A. M. Litke and E. J. Chichilnisky

JN 95:3311-3327, 2006. First published Jan 25, 2006; doi:10.1152/jn.01168.2005

J Neurophysiol 95: 3311–3327, 2006.
First published February 1, 2006; doi:10.1152/jn.01168.2005.

TRANSLATIONAL PHYSIOLOGY

Electrical Stimulation of Mammalian Retinal Ganglion Cells With Multielectrode Arrays

Chris Sekirnjak,[1] Pawel Hottowy,[2] Alexander Sher,[3] Wladyslaw Dabrowski,[2] A. M. Litke,[3] and E. J. Chichilnisky[1]

[1]*The Salk Institute for Biological Studies, San Diego, California;* [2]*Faculty of Physics and Applied Computer Science, AGH University of Science and Technology, Krakow, Poland; and* [3]*University of California, Santa Cruz, California*

Submitted 4 November 2005; accepted in final form 22 January 2006

Sekirnjak, Chris, Pawel Hottowy, Alexander Sher, Wladyslaw Dabrowski, A. M. Litke, and E. J. Chichilnisky. Electrical stimulation of mammalian retinal ganglion cells with multielectrode arrays. *J Neurophysiol* 95: 3311–3327, 2006. First published February 1, 2006; doi:10.1152/jn.01168.2005. Existing epiretinal implants for the blind are designed to electrically stimulate large groups of surviving retinal neurons using a small number of electrodes with diameters of several hundred micrometers. To increase the spatial resolution of artificial sight, electrodes much smaller than those currently in use are desirable. In this study, we stimulated and recorded ganglion cells in isolated pieces of rat, guinea pig, and monkey retina. We used microfabricated hexagonal arrays of 61 platinum disk electrodes with diameters between 6 and 25 μm, spaced 60 μm apart. Charge-balanced current pulses evoked one or two spikes at latencies as short as 0.2 ms, and typically only one or a few recorded ganglion cells were stimulated. Application of several synaptic blockers did not abolish the evoked responses, implying direct activation of ganglion cells. Threshold charge densities were typically <0.1 mC/cm^2 for a pulse duration of 100 μs, corresponding to charge thresholds of <100 pC. Stimulation remained effective after several hours and at high frequencies. To show that closely spaced electrodes can elicit independent ganglion cell responses, we used the multielectrode array to stimulate several nearby ganglion cells simultaneously. From these data, we conclude that electrical stimulation of mammalian retina with small-diameter electrode arrays is achievable and can provide high temporal and spatial precision at low charge densities. We review previous epiretinal stimulation studies and discuss our results in the context of 32 other publications, comparing threshold parameters and safety limits.

INTRODUCTION

Recent attempts to restore vision in the blind have met with extraordinary success. Electrical stimulation of retinas in people with neurodegenerative diseases has shown the potential for direct excitation of neurons as a means of re-establishing sight. Long-term retinal implants in several profoundly blind people were shown to produce perceptions of light and allowed for the detection of motion and discrimination of very simple shapes (Humayun 2003; Humayun et al. 2003).

Such achievement brings hope to the millions of people worldwide who suffer from photoreceptor loss because of advanced retinitis pigmentosa or age-related macular degeneration (Heckenlively et al. 1988; Klein et al. 1997). It is expected that 10 years from now, macular degeneration will become the single leading cause of legal blindness, with an incidence as high as 5.5% in people over 65 (Klein et al. 1997). While degenerative diseases result in severe damage to photoreceptors, inner retinal neurons survive at fairly high rates (Kim et al. 2002; Santos et al. 1997; Stone et al. 1992) and may be electrically excitable. The fundamental concept underlying retinal neuroprosthetic devices is to electrically activate those residual neurons by bypassing the damaged photoreceptors, thus achieving artificial vision in otherwise blind patients. Of several prosthetics designs, epiretinal implants specifically target ganglion cells by positioning electrodes in close proximity to the inner surface of the retina.

Despite recent successes, the current implants are but a first step toward restoring sight. To create useful vision, stimulating electrodes must be arranged in two-dimensional arrays that generate a visual image made up of a matrix of discrete perceptions of light. Psychophysical studies suggest that foveal implants may provide the user with an acceptable level of mobility if they contain a minimum of ~600 electrodes (Cha et al. 1992a,b). To achieve this number or greater, electrodes must be tightly packed, necessitating small stimulation sites. At present, a typical epiretinal implant contains tens of electrodes with diameters of a few hundred micrometers, spaced several hundred micrometers apart (Humayun 2003). Considering that such electrodes are much larger than the cells they stimulate, the need for implants with hundreds or thousands of much smaller electrodes is apparent. To match the intrinsic resolution of the visual system, an advanced implant would devote one electrode to every ganglion cell. This requires that each electrode be similar in size to a ganglion cell (~5–20 μm). Instead of affecting hundreds or thousands of cells, each electrode would evoke a few spikes in a few retinal ganglion cells.

The success of the next generation of implantable devices will be tied to our understanding of how to activate neurons with extracellular electric stimuli applied to the retinal surface through electrodes that approach cellular dimensions. Little is known about the parameters that would permit reliable retinal

Address for reprint requests and other correspondence: E. J. Chichilnisky, The Salk Institute for Biological Studies, 10010 N. Torrey Pines Rd., La Jolla, CA 92037 (E-mail: ej@salk.edu).

The costs of publication of this article were defrayed in part by the payment of page charges. The article must therefore be hereby marked "*advertisement*" in accordance with 18 U.S.C. Section 1734 solely to indicate this fact.

stimulation with small electrodes. When the electrode surface area is reduced, current density and charge density increase rapidly, and high charge densities are known to cause tissue damage by electrochemical reactions (Brummer et al. 1983; Pollen 1977; Tehovnik 1996). A detailed in vitro analysis of small electrode stimulation is thus a prerequisite for developing such implants for use in human patients.

A comprehensive literature review reveals that the feasibility of stimulation with arrays of small electrodes in mammalian tissue has not been adequately tested. The majority of studies involving retinal stimulation have used needle-shaped probes with one or two conductors at the end of an insulated rod, such as platinum wires or concentric microelectrodes. In its simplest form, such stimulating probes are made of metal wires several hundred micrometers in diameter, exposed at the tip and insulated elsewhere (Doty and Grimm 1962; Humayun et al. 1994; Nadig 1999; Suzuki et al. 2004; Weiland et al. 1999).

Others have attempted to use stimulating microprobes with tip diameters of 25 μm or smaller (Dawson and Radtke 1977; Jensen et al. 2003; Rizzo et al. 1997; Wyatt et al. 1994). However, the geometry of such probes differs greatly from the planar disk electrode design developed for current epiretinal implants. Stimulation, furthermore, is always limited to a single stimulation site, precluding the study of stimulation using multiple electrodes and their interaction effects.

The use of multielectrode arrays for retinal stimulation has been mainly limited to large electrodes with diameters between 100 and 1,500 μm (Greenberg 1998; Hesse et al. 2000; Humayun et al. 1999, 2003; Rizzo et al. 2003a; Walter and Heimann 2000). Multielectrode arrays with smaller electrodes ($\sim$10 μm diam) have been used to stimulate the retina in the subretinal space (Stett et al. 2000; Zrenner et al. 1999). Grumet has used an array to selectively stimulate the axons of retinal ganglion cells, using a separate distant array to record somatic spikes (Grumet 1999; Grumet et al. 2000). No study has targeted mammalian ganglion cell bodies for direct epiretinal stimulation using planar electrodes with surface areas $<$200 μm^2.

In this study, we established thresholds for stimulation of ganglion cells in rat, guinea pig, and primate retina using electrodes with surface areas of 30–500 μm^2 (diameters of 6–25 μm). We used these parameters to further study frequency dependence, pharmacology, and spatial interaction effects of stimulation. Our arrays use planar disk microelectrodes very similar to those used in present epiretinal prosthetics, but smaller by an order or two of magnitude. We conclude our analysis by discussing the results in the context of the pertinent literature.

Early and preliminary portions of this work have been presented elsewhere (Sekirnjak et al. 2006).

METHODS

Retinal preparation

This study used retinal tissue from 28 adult rats, 4 guinea pigs, and 1 macaque monkey. The average body weight was 289 ± 8 g for rats (Long-Evans), 386 ± 52 g for guinea pigs, and 4 kg for the macaque monkey (*Macaca radiata*).

Rodent eyes were enucleated after decapitation of animals deeply anesthetized with 10 mg/kg xylazine and 50 mg/kg ketamine HCl. Primate eyes were obtained from terminally anesthetized macaque monkeys used by other experimenters, in accordance with institutional guidelines for the care and use of animals. Immediately after enucleation, the anterior portion of the eye and vitreous were removed in room light and the eye cup placed in bicarbonate-buffered Ames' solution. Vitreous removal in rats was aided by a homemade extractor that allowed for rapid but gentle separation of retina and vitreous gel. The success rate for vitrectomies performed in this manner was 92%.

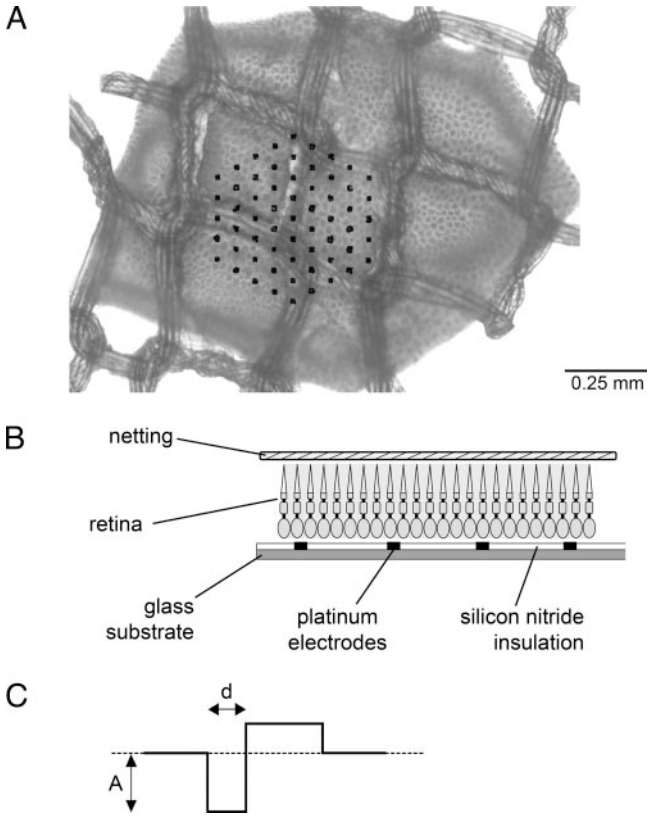

FIG. 1. Experimental design. *A*: a piece of retina positioned over the hexagonal multielectrode array (black dots) and held in place by nylon netting, photographed during a stimulation experiment. Electrode diameter = 14 μm. *B*: schematic cross-section of the retina–array assembly. Preparation is submerged in solution and grounded by a distant platinum wire. The 61 platinum electrodes are used both to record spike activity and to send current pulses. *C*: standard stimulus pulse used to stimulate ganglion cells.

Pieces of retina 1–2 mm in diameter (Fig. 1*A*) were separated from the retinal pigment epithelium and placed flat on the electrode array, with the ganglion cell layer facing the array (Fig. 1*B*). The tissue was held in place by weighted nylon netting positioned over the array. The preparation was mounted on a circuit board attached to an inverted microscope and continuously superfused at room temperature with Ames' solution bubbled with 95% oxygen and 5% carbon dioxide at a flow rate of 2–4 ml/min. Pharmacological agents (TTX, kynurenic acid, CNQX, AP-5, cadmium chloride) were added directly to the perfusion solution.

Multielectrode array

The array consisted of a planar hexagonal arrangement of 61 extracellular electrodes, $\sim 0.5 \times 0.5$ mm^2 in total size (Fig. 1*A*). These electrodes were used both to record action potentials extracellularly from ganglion cells (Chichilnisky and Baylor 1999; Meister et al. 1994) and to apply current to the tissue for stimulation. In some experiments, different neighboring electrodes were used for stimulating and recording.

The array was microfabricated on a glass substrate, with indium tin oxide leads and silicon nitride insulation (Litke 1998; Litke et al. 2003). Each electrode was formed by microwells (holes in the silicon

nitride layer), which were electroplated with platinum before an experiment (Fig. 1, *A* and *B*). This was accomplished by submersing the array in a 0.0025N HCl solution containing 1% chloroplatinic acid and 0.01% lead acetate and applying voltages of 1–5 V through 10-MΩ resistors for 10–120 s. Electrode size was determined by well diameter (5, 6, 8, 10, 12, or 14 μm) as well as the amount of platinum deposited in each well. Final electrode diameter varied between ~6 and 25 μm, with a fixed interelectrode spacing of 60 μm. The geometric electrode area (πr^2) was used to calculate current and charge densities; however, platinum tends to deposit in a granular fashion, rendering the effective electrode area significantly larger (Mathieson et al. 2004). A circular chamber glued on the glass plate allowed for perfusion of saline solution. A 4-cm-long platinum wire loop integrated into the chamber served as distant ground. All stimulations were performed using a monopolar configuration (electrode to distant ground).

Electrical stimulation and recording

Unless otherwise noted, experiments were performed on a setup allowing for simultaneous recording of all 61 electrodes and stimulation on multiple electrodes. The array was connected to a circuit board containing two custom-made readout application-specific integrated circuits (ASICs) that amplified, filtered, and multiplexed signals from the 61 electrodes and sent them to ADC cards installed in a PC. The board also contained two computer-controlled ASICs capable of sending current pulses to any configuration of electrodes (Dabrowski et al. 2005). A dim level of illumination was maintained during the entire experiment (room lights or microscope illuminator).

Recording and stimulation were controlled by interface software (Labview). Extracellular potentials were recorded from all 61 electrodes, digitized at 20 kHz (Litke 1999), and stored for off-line analysis. The available discrete stimulation pulse current amplitudes were 0.6, 0.8, 1.0, 1.2, 1.5, 1.7, 2.0, 2.3, 2.7,3.0, 3.3, 4.0, 4.7, 5.3, 6.0, 6.7, 8.0, 9.3, 10.7, 12.0, 13.3, and 16.7 μA (several threshold curves reported in Fig. 6*A* were determined using an earlier stimulus generator capable of delivering current amplitudes as low as 0.1 μA. This device was not used in subsequent experiments). The pulse consisted of a cathodic (negative) current pulse of amplitude A and duration d, followed immediately by an anodic (positive) pulse of amplitude $A/2$ and duration $2d$ (Fig. 1*C*). All pulses were individually calibrated to produce stimuli with zero net charge. Charge-balanced biphasic waveforms such as these minimize electrode corrosion by preventing charge accumulation and the associated irreversible Faradaic reactions (Merrill et al. 2005). Reported current values always refer to the negative phase amplitude A. Pulse duration was 0.05, 0.1, 0.2, 0.5, or 1 ms and always refers to the duration d of the cathodic phase. The pulse shape could be inverted in time to yield an anodic-first stimulus. Stimulation frequency was varied between 0.25 and 300 Hz.

Experimental protocol

Many ganglion cells show maintained activity under diffuse retinal illumination (Troy and Robson 1992) and fire spontaneous spikes in isolated pieces of retina. Stimulation on a particular electrode was typically attempted if spontaneous extracellular spikes could be recorded from that electrode. This approach guaranteed that the electrode was properly platinized and confirmed that ganglion cells in the vicinity of the electrode were alive. Typically, at least half of the platinized electrodes on an array showed spontaneous activity from at least one cell. Spontaneous spikes were readily distinguished from evoked spikes because they bore no temporal relationship to the stimulus pulse, whereas evoked spikes were locked to the stimulus onset.

Stimulation was typically attempted by using the lowest current settings and was then increased systematically if no response was seen. Threshold was defined as the current setting which produced a spike with nearly every stimulus pulse (≥90% of trials) while stimulating at 1–2 Hz. Latency was defined as the time between stimulus pulse onset and the first deflection of the evoked spike. Unless otherwise stated, threshold current, threshold charge, and threshold charge density always refer to the negative phase of the biphasic, charge-balanced stimulus pulse.

For pharmacological manipulations, a minimum drug perfusion time of 5–10 min was allowed before responses were recorded.

Data analysis

Multielectrode data were analyzed off-line using Labview, Matlab, and Igor Pro. Means, SE, and P values were calculated in Microsoft Excel. Images were processed in Adobe Photoshop.

Chronaxies were calculated by fitting power functions $y = a/x + b$ and $y = a/x^p + b$ (Holsheimer et al. 2000; Lapicque 1907; Ranck 1975) or exponentials $y = b/(1 - e^{-x/a})$ (Greenberg 1998; Lapicque 1907; Plonsey and Barr 1988) to the strength-duration data. The asymptote (coefficient b) was defined as the rheobase; chronaxie was calculated as $(a/b)^{1/p}$, a/b, or aln2 for power and exponential fit functions, respectively. Fit quality was assessed by calculation of χ^2 and visual inspection of the fit curve, and noticeably poor fits were not included in the analysis. Given the small number of data points available for some cells, the quality of the fit and resulting parameters differed for the individual functions, and thus values from all three are reported.

Autocorrelations of evoked and spontaneous spiking were obtained by generating histograms of spike times and interspike intervals, respectively. On average, ~37 spikes were used per histogram. Spontaneous histograms were aligned so that time = 0 coincided with the occurrence of the peak of the first evoked spike.

Power function fit lines to literature data and R^2 values were calculated in Igor Pro by fitting linear functions to the logarithmic plots of threshold parameters.

Statistical comparisons were done by performing a Student's t-test (2-tailed, equal variance) with a significance limit of $P < 0.05$.

Errors and error bars reported in this study are SE, unless otherwise stated.

Threshold artifact subtraction

To reveal spikes with latencies of <2 ms, a novel digital subtraction technique was used. Spikes obscured by the stimulation artifact (which typically lasted for several milliseconds) were made visible by increasing the stimulation current until a possible spike threshold was reached. Just below threshold, the recorded traces changed shape noticeably on about half of the stimulus trials (e.g., a change in curvature or peak height), indicating that a possible spike hidden inside the artifact was elicited on some trials (Fig. 2*B*). Subsequently, the digital difference between two such traces was calculated. Because the artifact itself was identical in both traces, the subtraction cleanly revealed the spike inside the stimulus artifact. Typically, several traces with and without a suspected spike were averaged before subtraction to increase the signal over the noise. This method necessitated recording the spikes on an electrode immediately adjacent to the stimulation electrode, because the signal recorded at the stimulation site usually saturated the amplifier and was not suitable for subtraction. The results obtained were comparable to or better than those reported for artifact suppression by local curve fitting (Wagenaar and Potter 2002).

We further verified this technique in six cells by applying TTX (1 μM) to the bath solution. The stimulus artifact recorded in TTX was subtracted from the traces containing obscured spikes. In these cells, the resulting subtracted spikes were identical to the spikes obtained using the above method. An example of this is shown in Fig. 4*A*.

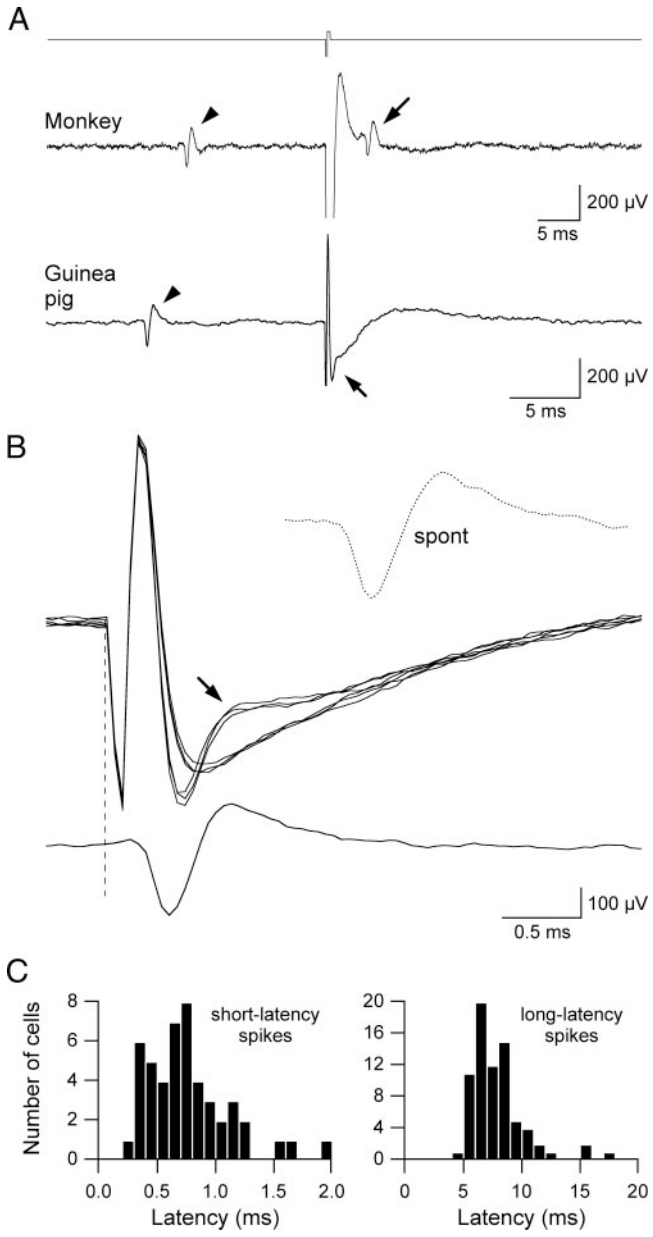

FIG. 2. Ganglion cell responses evoked by electrical stimulation. *A*: spontaneous spikes (arrowheads) and evoked spikes (arrows) in monkey and guinea pig retina. Stimulus pulse is shown above traces. Latency in the monkey cell was 5.6 ms, whereas the evoked spike in the guinea pig trace was obscured by the stimulus artifact and required digital subtraction to reveal. *B*: same cell as *bottom* of *A* at an expanded scale. Superposition of several stimulation trials is shown, some of which evoked a spike (arrow). Bottom trace is the digital subtraction of averaged traces from trials with and without an evoked spike. Dashed line indicates stimulation onset. Latency was 0.25 ms. *Inset* (*top right*): spontaneous spike from this cell at the same scale. *C*: spike latencies measured for 48 short-latency spikes (*left*) and 74 long-latency spikes (*right*) using 0.1-ms pulses.

Literature analysis

Data from epiretinal stimulation studies were compiled as follows. Threshold current, current density, charge, and charge density necessary to elicit a ganglion cell response were median or mean values as reported in each study. When a list of thresholds was reported, an average value was calculated; when a range of thresholds was reported, the minimum or the median value was used; in some cases, a "typical" value was taken from a representative example or figure. Whenever possible, a missing parameter was calculated from reported parameters, for instance, threshold current from reported threshold charge (Humayun et al. 1999; Suzuki et al. 2004), surface area from charge density (Dawson and Radtke 1977), or current from reported charge density (Nadig 1999). In a few cases it was not possible to calculate a parameter, and it was estimated from other publications by the same author or the same group (asterisks in Table 1). When such substitution was not possible, the study was not included (Benjamin et al. 1994; Crapper and Noell 1963; Kuras and Gutmaniene 1997; Narayanan et al. 1994). Several studies were represented by multiple entries when different values of parameters were reported (electrode size, duration, pulse shape) or when several drastically different results were reported for the same parameters (such as for 2 or more human subjects). The geometric surface area was calculated from the reported electrode geometry [circular or rectangular for planar electrodes: πr^2 or l^2, cylindrical for exposed wires: $\pi r^2 h$, conical for cone tips: $\pi r(r^2 + h^2)^{1/2}$, spherical for ball electrodes: $4\pi r^2$]. When two or more electrodes were reported to be coupled electrically and used simultaneously, the surface area was multiplied accordingly. When a stimulus consisted of high-frequency pulse trains, the effective pulse duration was taken as the number of pulses per train times the single-pulse duration (Laube et al. 2003; Walter and Heimann 2000). Whenever possible, data from normal animals, not those with degenerated retinas, were used.

For plotting the neural injury limit, cat cortical tissue data from McCreery et al. (1990) was fit to the equation $\log(Q/A) = k - \log(Q)$, where Q is the charge in nC and Q/A is the charge density in mC/cm^2 (Merrill et al. 2005; Shannon 1992). The data can be fit with a coefficient k varying between 1.7 and 2.0; both values were used for the injury limit plots in Fig. 12.

RESULTS

We electrically stimulated pieces of isolated mammalian retina while simultaneously recording spiking activity in ganglion cells. The properties of evoked spikes are presented first, followed by strength-duration relationships, temporal properties, and the results from multielectrode stimulation.

Stimulation at individual array electrodes resulted in all-or-none spikes recorded at latencies between a few hundred microseconds and tens of milliseconds. Of the 184 successfully stimulated ganglion cells, 165 were from rats, 11 were from guinea pigs, and 8 were from the monkey. On average, each retina yielded 6 ± 1 stimulated cells. Most responses consisted of one or two spikes, although in some cells later spikes were recorded.

Response latencies

We classified spikes with latency ≥2 ms as long-latency spikes and earlier responses as short-latency. Latencies >10 ms were infrequently observed, and virtually no spikes occurred >20 ms after stimulation onset. Typically, only long-latency spikes could be readily discerned because the stimulus artifact obscured the first few milliseconds of the recording.

Figure 2*A* shows two spontaneously firing ganglion cells and their responses to single stimulus pulses. While the primate cell (*top*) responded with a distinct spike at latency 5.6 ms, the guinea pig response (*bottom*) was obscured by the stimulus artifact. To isolate the evoked short-latency spike, a threshold artifact subtraction method was used (see METHODS). Briefly, the artifact was selectively eliminated by recording several traces near threshold and subtracting those traces that did not contain evoked spikes (Fig. 2*B*). This method was typically

used when a neighboring electrode was used for stimulation in lieu of the recording electrode, because this configuration reduced the artifact below amplifier saturation levels and allowed the artifact to be subtracted. The result for the guinea pig cell is shown at the bottom of Fig. 2*B*: a spike was revealed at 0.25 ms latency. For 86 spikes in rats, visible without artifact subtraction, the average latency was 7.6 ± 0.3 ms, whereas 48 artifact-subtracted spikes had a latency of 0.73 ± 0.05 ms. Nearly all short-latency spikes occurred at <1 ms; the shortest latencies recorded in this study were ~0.2 ms. Latency histograms for both short- and long latency spikes are shown in Fig. 2*C*.

Evoked spikes usually resembled the recorded spontaneous spikes, but occasionally spikes from a different cell were elicited. Short-latency spikes in particular tended to be of identical shape as the spontaneous spikes. This is shown in the *inset* of Fig. 2*B*: the evoked spike resembled the spontaneous spike. Two further examples are shown in Fig. 4*A* and in the *inset* to Fig. 7*B*. Of 48 subtracted short-latency spikes, 42 unambiguously matched the spontaneous spike.

To elucidate the origin of long-latency spikes, the method of digital artifact subtraction was applied to recordings which contained both short- and long-latency spikes. It seemed possible that each long-latency spike was in fact the second spike of a pair response and not a solitary spike. Indeed, analysis of 20 cells revealed that the occurrence of long-latency spikes (6.4 ± 0.3 ms) was always associated with short-latency responses (0.7 ± 0.1 ms). An example from guinea pig retina is shown in Fig. 3: whereas the raw data traces (Fig. 3*A*) showed only three long-latency spikes (asterisks), the artifact-subtracted traces (Fig. 3*B*) revealed that every long-latency spike was preceded by a short-latency spike at 0.35 ms. Furthermore, an analysis of spontaneous spiking activity showed that spike doublets spontaneously occurred in this cell. This is shown at the *bottom* of Fig. 3*B*: the autocorrelation histogram of spontaneous spikes showed a peak at a latency similar to that of the evoked long-latency spikes. Thus the evoked spikes occurred with timing expected from the spontaneous activity. A second example from rat retina is shown in Fig. 3*C* for a cell with long-latency spikes at 7 ms. Spike timing analyses were performed in a total of eight cells, with similar results: the spontaneous interspike intervals matched the typical intervals between short- and long-latency spikes. These results indicate that some cells responded to a single stimulus pulse with a spike pair, with the first spike obscured by the artifact, and that this tendency toward paired spiking was evident in the spontaneous activity of the cell.

The method of analyzing spike timing was further used to calculate the approximate latency of obscured short-latency spikes when only long-latency spikes were available. Figure 3*D* shows an example of a cell in which a large stimulus artifact precluded the use of the artifact subtraction method; only long-latency spikes were discernible. By aligning the peaks of the two histograms, a short-latency spike (dashed box) was inferred at times ≤1 ms. Similar results were found in three cells and suggest that short-latency responses can be deduced from the observance of long-latency spikes.

Last, we compared the spike latencies of long-latency responses evoked with stimulation electrodes of different diameters, which ranged from 6 to 25 μm in this study. No systematic difference was observed when large rather than small electrodes

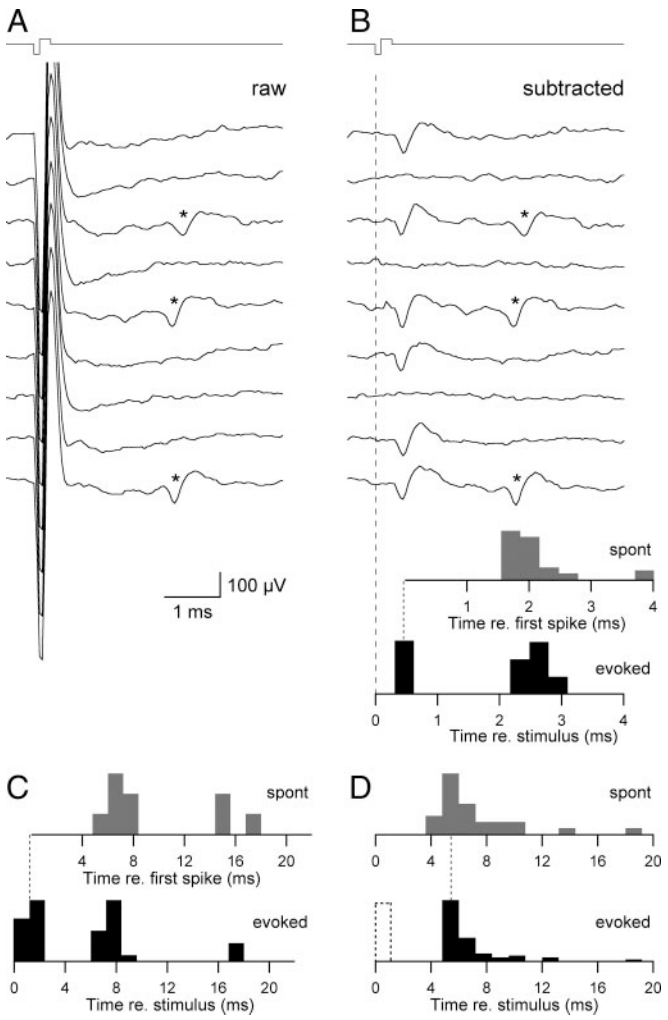

FIG. 3. Relationship between short- and long-latency spikes. *A*: raw traces of 9 stimulation trials in guinea pig retina near threshold. Stimulus pulse is shown above traces. Long-latency spikes (*) were evoked on several trials (latency 2–3 ms). *B*: *top*: artifact-subtracted traces revealed short-latency spikes (latency 0.35 ms), some of which were followed by long-latency responses. Dashed vertical line marks onset of stimulation. *Bottom*: latency histograms of spontaneous and evoked spikes. Spontaneous histogram plots interspike intervals and was offset in time by latency of early spikes. Bin width: 0.3 ms. *C*: latency histograms in another cell with long-latency responses at ~7 ms (rat). Bin width: 1.2 ms. *D*: latency data from a cell for which artifact subtraction was not possible and thus only the long-latency response (at 5 ms) was available (rat). Inferred short-latency spikes occurred at times indicated by dashed box. Bin width: 1.2 ms.

were used and average latencies for the smallest electrodes (6–9 μm) were similar to the largest (20–25 μm): 8.2 ± 0.7 and 7.1 ± 0.4 ms, respectively ($P > 0.2$; $n = 32$ cells).

Pharmacological manipulations

Several ion channel antagonists were applied to the perfusion solution to further study the evoked responses. To ascertain that the observed spikes were of neuronal origin, the sodium channel blocker TTX (1 μM) was added to the perfusion solution. In 3 guinea pig and 17 rat cells, all spikes (both spontaneous and evoked) disappeared within seconds of drug application, confirming their identity as neuronal action potentials. An example is shown in Fig. 4*A*: application of TTX eliminated evoked short-latency spikes, leaving only the pulse artifact. When this artifact

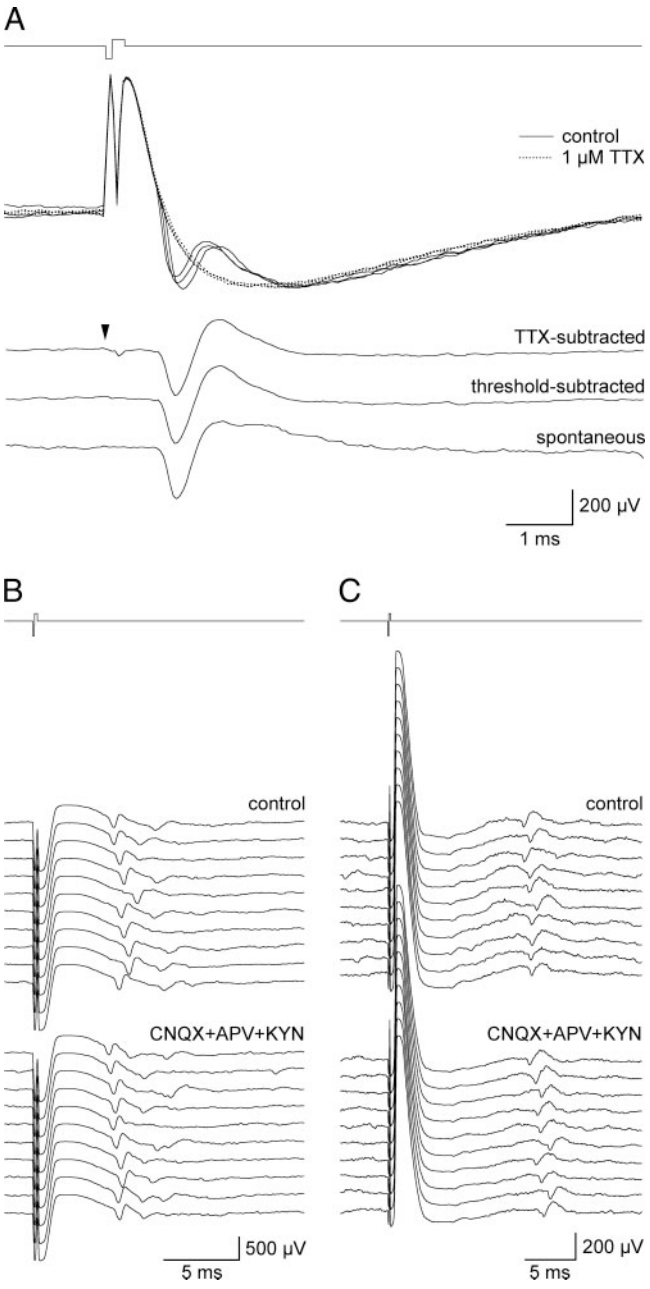

FIG. 4. Pharmacological manipulations. *A*: *top*: responses evoked by a 1-μA pulse (solid traces) were eliminated by application of TTX (dotted traces). A superposition of 3 trials is shown for each condition. *Bottom*: spikes obtained by subtracting the TTX response from control (1st trace), by using threshold artifact subtraction (2nd trace) and a spontaneous spike (3rd trace). Arrowhead marks onset of stimulation; latency = 0.8 ms. *B* and *C*: *top*: responses to 10 stimulus pulses in a cell with spikes at latency 5.5 ms (*B*) and in a cell with spikes at 15 ms (*C*) in rat retina. A combination of glutamate receptor antagonists (CNQX, APV, kynurenic acid) added to the perfusion solution (bottom traces) failed to eliminate responses.

was subtracted from the control responses, an evoked spike was revealed (Fig. 4*A*). The waveform of this spike did not differ from that derived by threshold artifact subtraction or the spontaneous spike recorded at this electrode (Fig. 4*A*, *bottom*). Similar results were found in five cells.

To study whether the applied current pulses acted directly on ganglion cells or involved more distant cells with synaptic connections to the recorded cell, blockers of synaptic transmission were added to the perfusion solution. A combination of the following agents was used: the broad spectrum glutamate antagonist kynurenic acid (1 mM), the *N*-methyl-D-asparate (NMDA) receptor blocker APV (400 μM), and the AMPA-receptor blocker CNQX (75 μM). These blockers have been used in retinal preparations by other groups at equal or lower concentrations (Jensen et al. 2005a; Stett et al. 2000; Ziv et al. 2002). Figure 4, *B* and *C*, shows examples of responses from two cells, recorded before and after addition of the blockers. Spike shapes, latencies, and response rates were unchanged, even in the cell with spikes at latency 15 ms (Fig. 4*C*). No systematic differences between spikes elicited in control and drug conditions were observed in any of nine cells. These findings suggest that ganglion cells were activated directly, not trans-synaptically, and further corroborate the notion that apparent long-latency spikes (such as in Fig. 4, *B* and *C*) are not solitary spikes, but part of a two-spike response.

In separate experiments, the calcium channel blocker cadmium chloride (100–250 μM) was applied to the perfusion solution to abolish synaptic transmission (data not shown). In 10 cells, evoked spikes were still observed after drug application, indicating that the observed spikes were not produced by mechanisms involving calcium-dependent synaptic transmission.

Minimal thresholds and spatial spread

Spikes were evoked in ganglion cells using currents between 0.6 and 5 μA. When stimulated with 0.1-ms pulses, the average threshold current for 78 rat cells stimulated under similar conditions was 0.81 $\pm$ 0.03 μA, corresponding to a charge of 81 $\pm$ 3 pC and a charge density of 0.073 $\pm$ 0.005 mC/cm^2. Electrode diameter ranged from 6 to 25 μm, and we present an analysis of thresholds as a function of electrode size below (see Fig. 10). In many cases, the lowest current setting of our stimulator (0.6 μA) yielded a superthreshold response, indicating that the reported average thresholds may be overestimated.

Thresholds were lowest when the recording electrode, rather than a neighboring electrode, was also used for stimulation. To examine whether spikes could be elicited by stimulating at a distance from the recording site, electrodes immediately adjacent to the recording electrode were used to stimulate. Figure 5*A* shows average results for eight cells, stimulated with one, three, or six adjacent electrodes (electrode diameter 15 $\pm$ 2.6 μm). The goal was to elicit the same long-latency spike using the different configurations of stimulation sites shown. Thresholds for spike initiation increased several-fold, depending on the number of active electrodes. In particular, when a single neighboring electrode was used for stimulation, about 3 times more current was needed compared with stimulation at the recording electrode. This indicates that a resolution of the order of the electrode spacing or finer ($\leq$60 μm) can be achieved with minimal threshold stimulation.

The preceding results suggest that stimulation using low stimulus amplitudes ($<$0.1 mC/cm^2) usually affected only cells in the vicinity of the stimulation electrode. To further verify this, in 35 low-amplitude stimulation experiments (average charge density 0.071 $\pm$ 0.004 mC/cm^2, electrode diameter 12.7 $\pm$ 0.5 μm), all electrodes surrounding the stimulation electrode were inspected for evidence of evoked spikes which

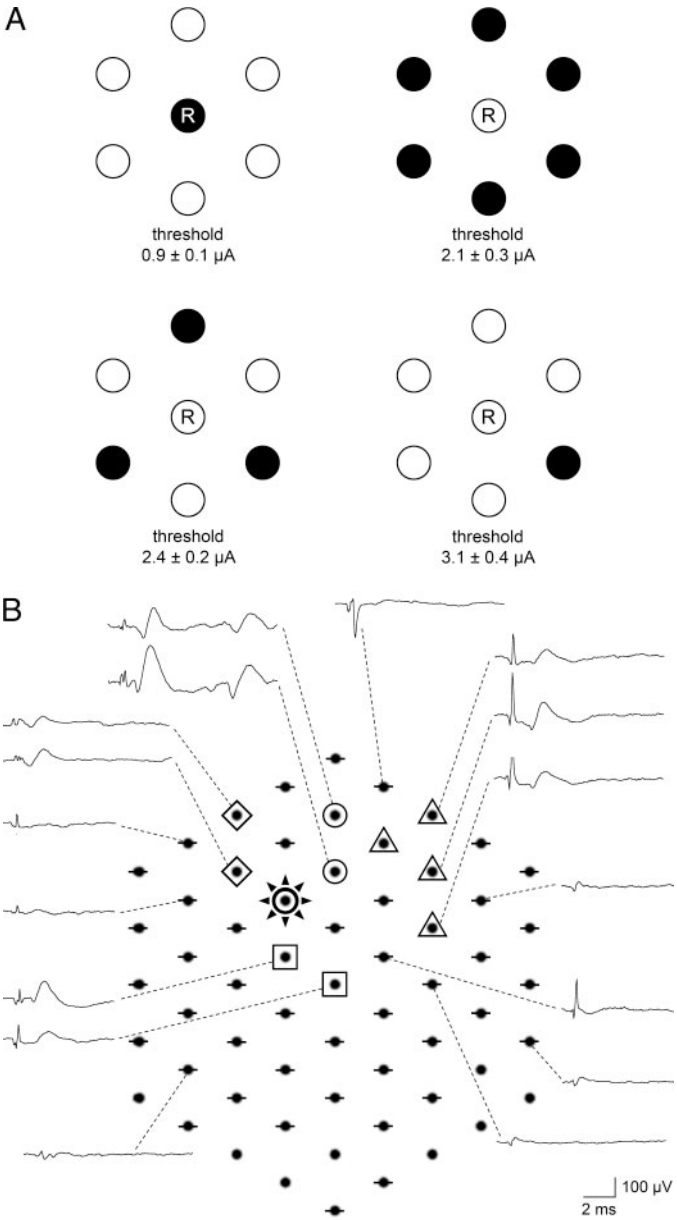

FIG. 5. Spatial spread of stimulation. *A*: spike thresholds for several stimulation configurations. Region adjacent to the center recording electrode (R) on the hexagonal array is shown, with filled circles indicating active electrodes used for stimulation, and open circles denoting unused electrodes. All active electrodes were stimulated simultaneously and at the same current amplitude. In addition to the standard setup (*top left*), 3 alternative configurations were tested: all neighboring electrodes, 3 electrodes, and a single neighboring electrode. Threshold currents are shown as averages over 8 cells and indicate lowest value found when multiple electrode combinations were tested. Corresponding charge densities were 0.09, 0.22, 0.25, and 0.32 mC/cm^2. Electrodes were 60 μm apart. *B*: spikes evoked by a strong stimulus (0.35 mC/cm^2) delivered through the electrode marked with the large radiating symbol. After application of TTX, the artifact was subtracted for each electrode individually. Spikes from 4 cells were detected (circles, triangles, squares, and diamonds), while most electrodes showed no evoked spikes (horizontal lines through electrodes). Empty electrodes were not tested. Traces are examples of TTX-subtracted signals recorded at sites indicated. Fast early deflections are stimulus artifacts; slower deflections are spikes. Scale was the same for all traces.

differed in latency, shape, or reliability from the ones recorded on the center electrode. Such additional spikes would indicate recruitment of neurons at nearby locations. Of 186 neighboring electrodes analyzed for long-latency spikes, only 1 showed an additional evoked spike. However, additional evoked spikes were frequently seen on surrounding electrodes when the current was increased several-fold, suggesting recruitment of cells tens of micrometers distant, consistent with the results shown in Fig. 5*A*. Still higher currents sometimes elicited spikes on non-neighboring electrodes, >150 μm away from the stimulation electrode.

To further investigate spatial spread of activation, a more detailed analysis was performed to detect short-latency spikes around the stimulation electrode. In four experiments, we applied TTX and subtracted the averaged stimulus artifact on each electrode individually to reveal additional short-latency spikes, as in Fig. 4*A*. In two such experiments with a stimulus strength of ~0.1 mC/cm^2 (electrode diameter 10 μm), no short-latency spikes were found outside the 60 μm radius around the stimulation electrode. In two further experiments stimulated at 0.21 and 0.35 mC/cm^2 (electrode diameters 7 and 6 μm), spikes were detected as far away as 160 μm. One example of strong-stimulus stimulation is shown in Fig. 5*B*: while the majority of electrodes on the array recorded no evoked spikes, four separate responses were elicited in the vicinity of the stimulation site. The spikes from these stimulated cells were each detected on two or more electrodes and the electrode recording the largest spike amplitude can be used to infer the approximate location of the soma. Most evoked spikes (circles, squares, diamonds) were recorded within 60 μm of the stimulation electrode, but one cell was detected nearly 160 μm away (triangles). These results show that the radius of stimulated ganglion cells can be controlled by adjusting the stimulus strength.

The above results were obtained by applying cathodic-first pulses (Fig. 1*C*). For most cells, thresholds were slightly higher when the anodic phase was delivered first: in 18 cells stimulated with 0.05- or 0.1-ms anodic-first pulses, spike thresholds were 115 ± 5% of the thresholds measured using cathodic-first pulses.

Strength-duration relationship

The current required to elicit a spike depended strongly on pulse duration. In all three species tested, higher currents were required to evoke a spike when shorter pulses were applied. Durations were varied from 50 μs to 1 ms and several resulting strength-duration curves are shown in Fig. 6*A*. In the examples plotted here, electrode diameter, stimulation configuration, and spike latency differed considerably across cells, resulting in a wide spread of threshold curves. Nevertheless, the slopes of these curves were similar in monkey, guinea pig, and rat, indicating that the threshold-duration relationship was independent of the species.

To characterize each strength-duration curve by a time constant and an asymptote, power functions or exponentials were fit to the data (see METHODS). Rheobase is defined as the asymptote of the fit curve (Loeb et al. 1983; Ranck 1975) and chronaxie, the classical measure of responsiveness of a neuron, as the duration at which the threshold current is twice the rheobase (Lapicque 1907). The average chronaxie of 34 cells such as those shown in Fig. 6*A* was 407 ± 45 μs for 1/x fits, 338 ± 81 μs for power fits, and 212 ± 28 μs for exponential fits. The average rheobase was 0.51 ± 0.12, 0.60 ± 0.11, and

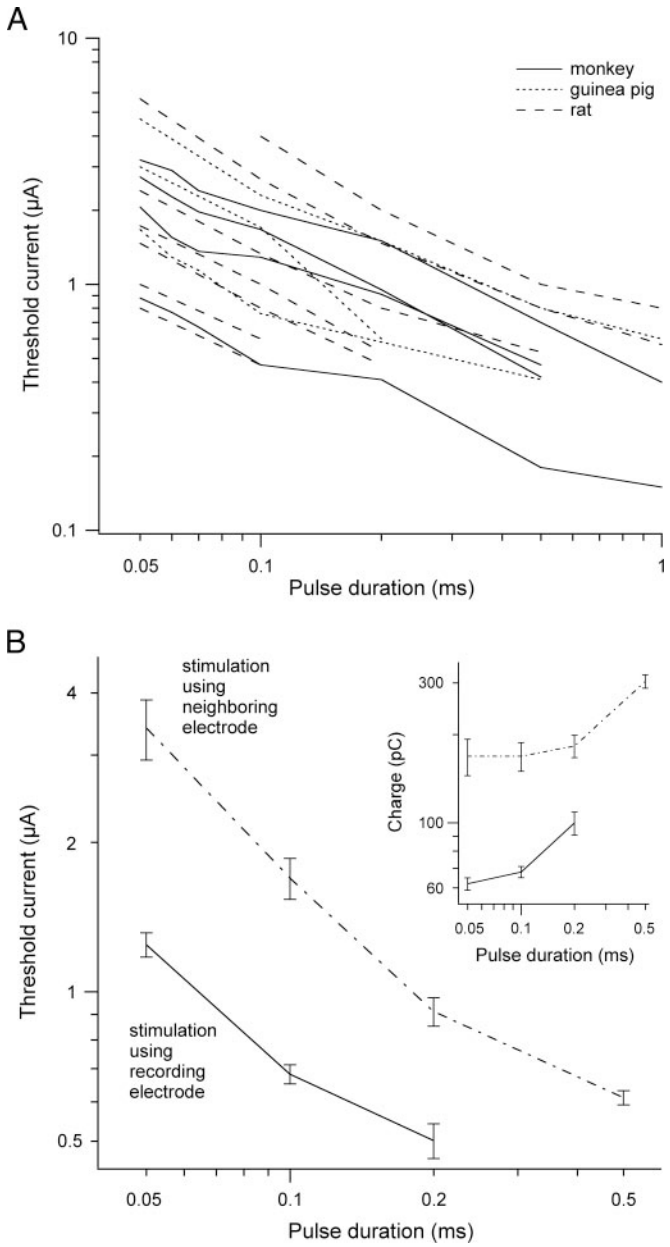

FIG. 6. Strength-duration curves. *A*: current required to elicit a spike is plotted as a function of stimulus pulse duration for several individual ganglion cells from monkey (solid lines), guinea pig (dotted lines), and rat (dashed lines). Several monkey and guinea pig cells shown here were stimulated using a pulse generator capable of delivering current pulses below 0.6 μA. *B*: threshold current and charge in rat retina. Average thresholds of 25 cells recorded under identical conditions are plotted against pulse duration. Two configurations are shown: stimulation at the recording electrode (solid line, 13 cells) and stimulation at an electrode adjacent to the recording site (dashed line, 12 cells). *Inset*: corresponding threshold charge for the same 2 configurations.

0.76 ± 0.16 μA, respectively. Fit quality was generally highest for power fits. Seven cells were from monkey, 7 from guinea pig, and 20 from rat, and all responses were long-latency spikes. When the group of 20 rat cells was divided into those stimulated with the recording electrode and those stimulated at a neighboring site, no difference in chronaxie was found ($P > 0.5$).

To facilitate comparison of thresholds in a single species and to show the influence of stimulation electrode position, Fig. 6*B* shows averaged data from 25 ganglion cells in rats. The cells were stimulated under identical conditions using electrodes with similar diameters (average 10.6 ± 0.5 μm). The solid line plots thresholds for stimulation at the recording electrode (13 cells), while the dashed line shows results from stimulation at a neighboring electrode (12 cells). As in Fig. 5*A*, eliciting a spike required several-fold higher currents when the site of stimulation was at an adjacent electrode. Because the charge delivered during the cathodic phase of the pulse is often used as a measure for stimulation strength, the *inset* plots the corresponding charge thresholds: charges were consistently <200 pC for pulse durations up to 0.2 ms, corresponding to charge densities <0.22 mC/cm^2.

To further corroborate the above notion that short- and long-latency spikes constitute doublet responses, we measured strength-duration curves of responses with latencies <2 ms. The average strength-duration relationship in 14 cells with short-latency spikes (latency 0.69 ± 0.08 ms) was similar to that of long-latency responses: chronaxies determined from fit curves (as above) were 571 ± 149, 299 ± 52, and 311 ± 113 μs; none of these values was significantly different from long-latency chronaxies ($P > 0.1$; $n = 45$ cells). These results suggest that the same neuronal element was excited in both short- and long-latency responses.

Frequency dependence

To mimic natural spike trains, a retinal implant must be capable of delivering pulses and evoke spikes at a wide range of stimulation frequencies. Furthermore, continual stimulation at higher frequencies may be a requirement for generating sustained percepts of light. We tested stimulation at pulse frequencies of up to several hundred hertz.

To examine high-frequency responses, two closely spaced pulses were applied, with the interpulse interval corresponding to frequencies of up to 200–300 Hz. High-frequency stimulation was deemed successful when spikes were evoked after the second stimulus pulse. Pulse pairs were applied for 10–20 s at intervals of 0.5 s and at stimulus strengths of about twice threshold. In nine cells tested, spikes were evoked on the second pulse on 99 ± 1% of trials at 100 Hz and 94 ± 4% at 200 Hz. Three cells were stimulated with 300-Hz pulse pairs and all responded at >90% of trials. All responses were short-latency spikes (latency 0.8 ± 0.2 ms). Data from such an experiment is shown in Fig. 7*A*: a superthreshold 300 Hz pulse pair reliably produced two short-latency spikes, more clearly seen in the artifact-subtracted traces shown below. A superposition of several stimulus trials is shown to demonstrate repeatability. In four cells, TTX was added to the bath solution to facilitate artifact subtraction and spike detection (data not shown).

To test responses to brief periods of sustained high-frequency stimulation, nine cells were continuously stimulated for 5–20 s at frequencies of up to 100 Hz. Figure 7*B* shows an example of responses to over 70 stimulus pulses near spike threshold, delivered at 32 Hz. Short-latency spikes were evoked on roughly one-half of the trials (arrow) and were used to subtract the artifact (*inset*). Thirty-two-hertz stimulation evoked spikes indistinguishable from those produced by 2-Hz stimulation or spontaneous activity.

Response rates, defined as the number of evoked spikes in a stimulation period, were measured at sustained pulse frequencies of up to 100 Hz at stimulus strengths of about twice threshold (Fig. 7*C*). Short-latency spikes (closed symbols) showed a slight reduction of the response rate at 50 Hz (<20%) and a significant drop at 100 Hz. We also observed a gradual reduction in spike amplitude throughout the stimulation period at frequencies above about 32 Hz (data not shown). Strikingly, long-latency responses (open symbols) were robust only up to 5 Hz and virtually no spikes were observed above 10 Hz. This observation was corroborated in one cell with a short-latency spike (0.7 ms), which was followed by a spike at latency 5 ms: stimulation at low frequencies consistently evoked both responses, while only the short-latency spike was observed at frequencies above 8 Hz.

We conclude that short-latency spikes can be reliably evoked in ganglion cells at pulse frequencies up to about 50 Hz and that late spikes are suppressed at moderate frequencies.

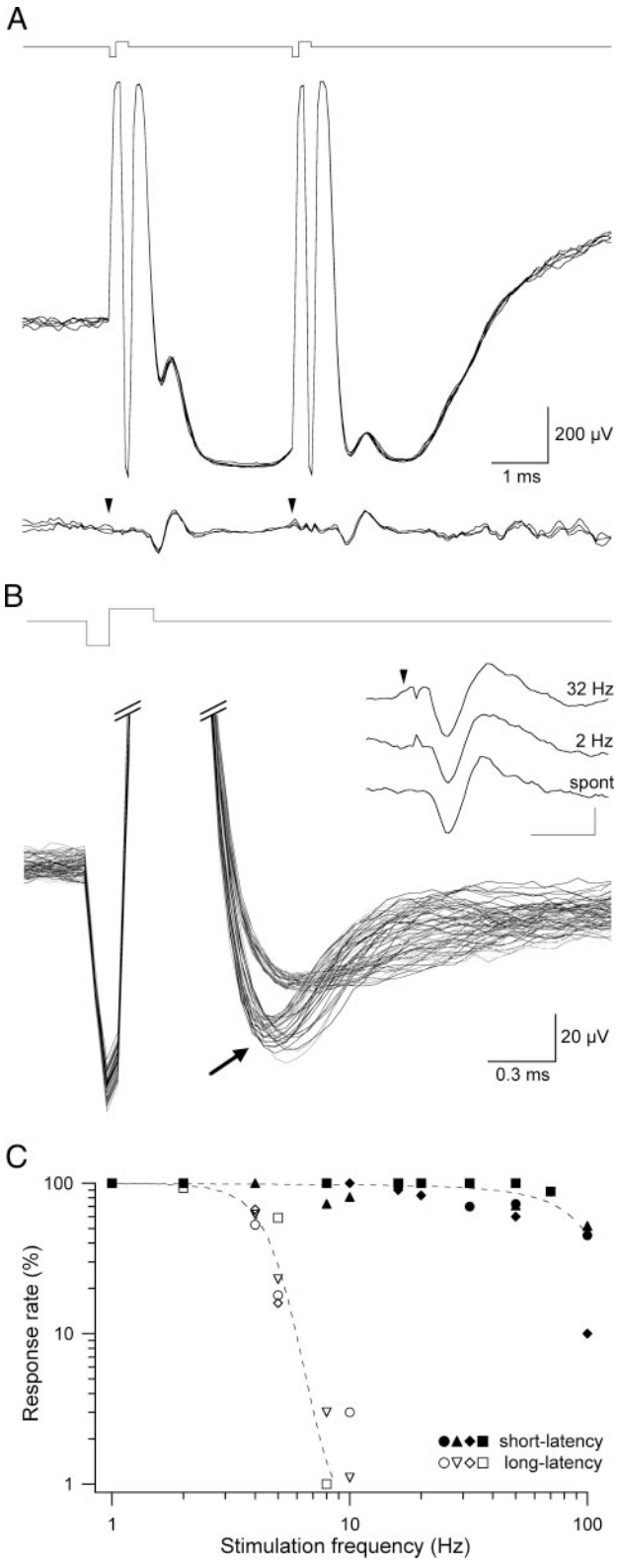

FIG. 7. Frequency dependence of stimulation. *A*: *top*: superthreshold responses to 300-Hz pulse pairs, applied every 500 ms in rat retina. Several superimposed trials are shown. *Bottom*: artifact subtraction revealed spikes at latency 0.75 ms. Arrowheads indicate stimulation onset. Spike-free traces necessary for artifact subtraction were obtained by decreasing the interval between pulse pairs until failures were observed. *B*: responses to sustained stimulation at 32 Hz near threshold in a different cell. A superposition of 73 trials is shown, about half of which evoked a spike (arrow). *Inset*: artifact subtraction of averaged traces shows evoked spike at latency 0.4 ms, along with the subtracted spike for low-frequency stimulation, and a spontaneous spike. Arrowhead indicates stimulation onset. Scale bar, 1 ms and 20 μV. *C*: percent evoked spikes (response rate) for spikes with latency 0.6 ± 0.1 ms (4 cells, closed symbols) and spikes with latency 9.1 ± 1.5 ms (4 cells, open symbols) for sustained stimulation at up to 100 Hz. Dashed lines are sigmoidal fits to data.

Sustained stimulation

Chronic retinal implants must be capable of delivering effective stimulation pulses over a period of many hours each day. To determine whether sustained low-frequency stimulation could reliably evoke spikes, we extended our stimulation period to the longest duration that was experimentally feasible.

Two cells were continuously stimulated for 30 min and two additional cells for 4.5 h. The longest sustained stimulations were performed using 0.8-μA pulses with 0.1-ms duration, delivered at frequencies of 1–2 Hz, and corresponding to a charge density of about 0.04 mC/cm^2 per pulse (electrode diameter 16 μm). Figure 8 shows an example of spikes evoked before and after a 4.5-h stimulation period: the cell showed robust responses after having been stimulated with over 16,000 pulses. A slight increase in threshold and spike latency (~20%) was noted at the end of the stimulation period.

Multielectrode stimulation

To generate artificial vision, a functional retinal implant requires independent activation of many closely spaced electrodes. To study responses to spatial stimulation patterns, the multielectrode array was used to stimulate at several electrodes simultaneously. Our goal was to show that simultaneous activation of two or more nearby electrodes did not influence each other. If that were the case, spikes elicited during multielectrode stimulation should not differ in threshold, shape, or number from individual stimulations.

We selected seven sites that clearly showed evoked long-latency spikes when stimulated individually. These evoked spikes differed in spike shape and latency, but had similar thresholds. All seven electrodes were subsequently activated simultaneously using 0.8-μA pulses (0.1-ms duration). Figure 9*A* shows spikes evoked at these sites and their locations on the

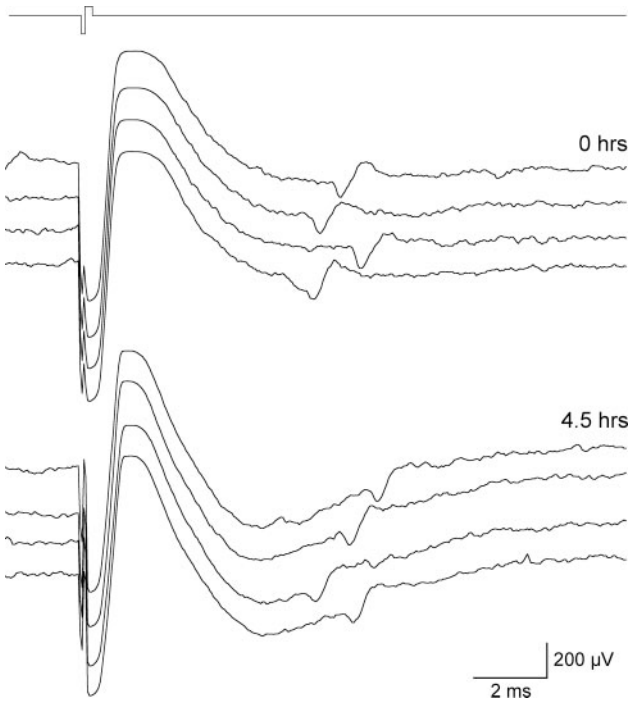

FIG. 8. Continuous low-frequency stimulation. Example of spikes evoked at the beginning (top traces) and at the end of a 4.5-h stimulation period with 0.8-μA pulses (0.1 ms, 1 Hz). Four response traces are shown for each time-point.

array. Simultaneous stimulation evoked seven distinct responses on seven spatially disparate electrodes.

To establish that the spikes evoked by simultaneous stimulation did not differ from those evoked by individual stimulation, traces recorded at each electrode under both conditions were compared. Two examples are shown in Fig. 9*B*: individually evoked spikes (single) were identical to simultaneously evoked spikes (all) for both electrodes shown here. Furthermore, Fig. 9*B* shows that stimulation at neighboring electrodes evoked independent responses. While this was expected given the low currents used here (see Fig. 5*A*), these data clearly establish that adjacent electrodes (1 and 2) did not influence each other during simultaneous stimulation. Only a small-amplitude deflection was recorded on electrode 1 at the latency of the spikes seen on electrode 2 (arrowhead), indicating that the cell stimulated by electrode 2 was probably located close enough to electrode 1 to be recorded as small spikes. To further ensure spatial precision, all 22 inactive electrodes surrounding the 7 active stimulating electrodes were inspected for spikes. While four adjacent electrodes showed small spikes that were recorded on one of the seven stimulation electrodes, none recorded new spikes.

Multielectrode stimulation was performed five times using various electrode arrays and spatial patterns, with results very similar to the data presented above. We conclude that evoking independent spikes on multiple electrodes spaced 60 μm apart is feasible with minimal cross-electrode interaction.

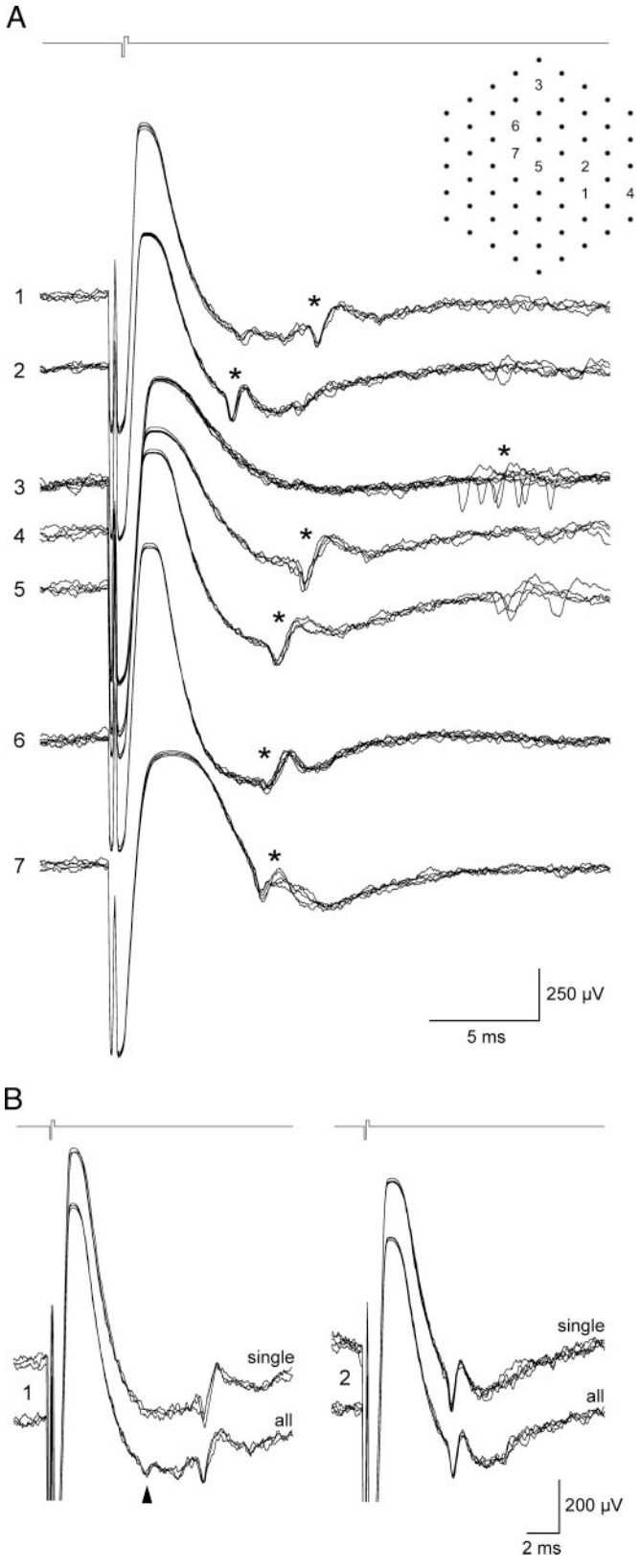

FIG. 9. Multiple site stimulation. Rat retina was stimulated at 7 electrodes simultaneously with 0.8-μA pulses. *A*: overlay of several trials is shown for each electrode (1–7) and evoked long-latency spikes marked with an asterisk. *Inset* (*top right*): location of active electrodes on the array. Latencies ranged from 5 to 18 ms. *B*: traces from neighboring electrodes 1 (*left*) and 2 (*right*). For comparison, spikes are shown for individual stimulation at only that electrode (single) as well as when all 7 electrodes were active (all). Evoked spikes showed no difference. Arrowhead indicates that the large spikes seen on electrode 2 were visible on electrode 1 as small deflections.

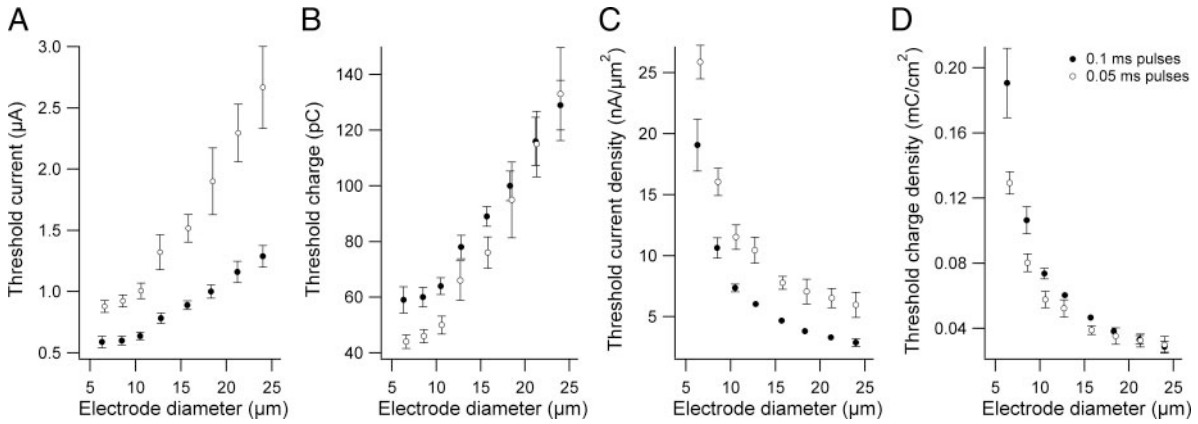

FIG. 10. Dependence of thresholds on electrode size. Thresholds were plotted against electrode diameter for 78 rodent cells stimulated with 0.1-ms pulses (●) and 59 cells stimulated using 0.05-ms pulses (○). Averages in bins of 2–3 μm are shown. *A*: current. *B*: charge. *C*: current density. *D*: charge density. Each is plotted for the same set of data. A single electrode was used for both stimulation and recording, and all responses were long-latency spikes. Error bars were omitted when SE was smaller than symbol size.

Electrode size

This study used arrays with electrodes that varied in diameter between 6 and 25 μm. To determine the influence of electrode size on thresholds, stimulation results were compared in a set of 86 cells for which the exact platinum disk diameters of the stimulating electrode was measured. Figure 10 shows thresholds as a function of electrode diameter, both for cells stimulated using pulse durations of 0.1 and 0.05 ms. Current, charge, current density, and charge density are plotted. All spikes were long-latency spikes (average 7.6 ± 0.3 ms).

Threshold current and charge (Fig. 10, *A* and *B*) increased by a factor of 2–3 between the smallest and the largest diameters, indicating that with smaller electrodes, less current and charge injection was necessary to elicit spikes in ganglion cells. Conversely, current density and charge density (Fig. 10, *C* and *D*) was drastically decreased for electrodes >10–15 μm. Note that the lowest threshold values plotted here may have been overestimated because the minimal available current setting (0.6 μA) often evoked a superthreshold response.

DISCUSSION

This study used dense arrays of small-diameter electrodes to electrically stimulate rat, guinea pig, and primate retina. We described the responses of individual ganglion cells to a wide range of pulse configurations and spatial stimulation patterns and showed that effective stimulation is feasible with high temporal and spatial precision. Our findings imply that the electrode size of future epiretinal prosthetics may safely approach the cellular dimensions of retinal ganglion cells.

Evoked spikes

Long-latency spikes (>2 ms) were readily observable, whereas spikes with shorter latencies could only be observed with digital artifact subtraction. Note that this classification into "short" and "long" latencies differs somewhat from that of other researchers: Jensen et al. (2005b) defines short as 3–5 ms and long as ≥9 ms; Stett et al. (2000) classifies spikes at latencies 1–10 ms as early and spikes at 10–20 ms as delayed. The definition of Crapper and Noel (1963) is more similar to the one used in this study: immediate spikes were defined as those around 0.5-ms latency and later responses as 5–15 ms.

EARLY SPIKES. The earliest observed responses occurred within several hundred microseconds of stimulation onset and probably represent the immediate activation of the ganglion cell spike generator. Actual latencies are in effect shorter than the reported values by 50–100 μs because of a delay introduced by the amplifier circuitry. Furthermore, if measured from the termination of the cathodic phase, true minimal latencies observed in this study amount to 50–150 μs. While these values are lower than the latencies in many studies, submillisecond spikes have been reported by a few authors (Crapper and Noell 1963; Grumet et al. 2000).

LATE SPIKES. We showed that evoked spikes at longer latencies are preceded by short-latency spikes. Long-latency spikes can thus be used to infer short-latency spikes even when the magnitude of the pulse artifact confounds direct observations of early spikes. However, it is possible that thresholds for long-latency spikes are systematically overestimated, because short-latency responses typically occur at lower stimulation currents than doublet responses.

Multispike responses are consistent with known intrinsic firing properties of ganglion cells, in which doublets or triplets in spike trains occur with interspike intervals of several ms (Devries and Baylor 1997). In our study, interspike intervals ranged from 4 to 16 ms, with the majority of long-latency spikes occurring ~5–7 ms after the short-latency spikes. We favor the interpretation of long-latency spikes as part of a doublet response over other suggestions such as conduction delays (Jensen et al. 2005b) or intracellular charging mechanisms for the following reasons: the small electrodes and currents used here make activation several millimeters from the recording site exceedingly unlikely; in each case tested, every long-latency spike was preceded by a short-latency spike; and earlier studies have not employed artifact subtraction methods, thus seeing only later spikes. Furthermore, long-latency spikes are only observed at stimulation frequencies <10 Hz, suggesting that higher repetition rates suppress multispike bursts.

Stimulation thresholds

SAFETY OF STIMULATION. An important prerequisite of implantable stimulators is their capability to deliver current that is safe, yet efficient. Unsafe stimulation can originate from two sources: electrochemical destruction of the stimulating electrode (such as corrosion) and neural tissue damage induced by toxic products near the electrode or by neuronal hyperactivity. Several electrochemical safety limits have been proposed, such as the often-stated nongassing limit of 0.3–0.4 mC/cm^2 for platinum electrodes (Brummer and Turner 1977). More recently, limits as low as 0.1 mC/cm^2 for cathodic stimulation with platinum electrodes have been recommended (Rose and Robblee 1990). Thresholds for tissue injury in cortex have been shown to arise from the synergistic interaction between charge and charge density: as the charge is increased, the charge density for safe stimulation decreases (McCreery et al. 1986, 1990; Merrill et al. 2005). The data of McCreery et al. show that no histologically detectable damage is produced with low-charge stimulation (<50 nC) even when the charge density is >1 mC/cm^2, whereas for pulses delivering a higher charge (1 μC), the damage threshold is <0.1 mC/cm^2. In the absence of detailed threshold measurements, concerns have been raised regarding the feasibility of using small-diameter electrodes in human patients, because they have been suggested to require much higher charge densities for threshold stimulation than large electrodes (Brummer et al. 1983; Greenberg 1998; Loeb et al. 1983). However, we found in this study that threshold stimulus pulses are characterized by low currents (~1 μA), low charge injection (~100 pC), and low charge densities (~0.1 mC/cm^2) despite the small electrode size. Several cells had threshold charge densities of <0.03 mC/cm^2, an order of magnitude lower than the platinum electrode safety limit. Furthermore, while we have used the geometric electrode area to calculate current and charge densities, the effective electrode area likely was significantly larger. Electroplated platinum tends to deposit in granular surface structures that greatly increase the area of metal in contact with the solution. It has been reported that the fractal-like platinum deposits can increase the surface area by up to 100 times (Kim and Oh 1996; Mathieson et al. 2004). Thus all density values reported here should be considered upper limits, further reducing the likelihood of electrochemical electrode damage.

Our results complement data recently reported for small-diameter needle electrodes, which have described threshold charge densities between 0.15 and 0.3 mC/cm^2 (Jensen et al. 2003; Rizzo et al. 1997; Wilms et al. 2003; Wyatt et al. 1994).

DISTANCE BETWEEN ELECTRODE AND CELLS. One factor contributing to the low thresholds in this study is the tight contact between electrodes and tissue. This was a requirement in our experiments because extracellular spikes cannot be recorded without close juxtaposition of the retina to the array. Novel techniques to minimize the gap between retina and epiretinal implant are being developed (Johnson et al. 2004; Schanze et al. 2002) and may ensure close contact in future prosthetic devices.

OPTIMAL ELECTRODE SIZE. We observed lower threshold current and charge for the smaller electrodes in this study than for the larger ones (see Fig. 10). However, the resulting charge density is increased for smaller electrodes. As electrode diameter drops below about 10 μm, the decrease in surface area outweighs the current decrease. It has been suggested that for electrodes smaller than the cellular size (~10 μm), the electric field is concentrated in too small an area for effective stimulation (Palanker et al. 2004). Thus electrode diameters around 10–15 μm may be the optimal size for selective single cell stimulation and might be an ideal compromise between excellent spatial resolution and high charge density. This size range would also have less stringent requirements on the distance between electrode and cells, since stimulation with <10 μm electrodes is disproportionately more sensitive to this distance (Palanker et al. 2004). Clearly, this issue will need to be readdressed once technical advances in retinal prosthetics call for even smaller electrodes as the ratio of electrodes to ganglion cells approaches 1.

SPATIAL RESOLUTION. One consequence of the low required stimulation strengths was the exceedingly localized nature of stimulation: excited cells were limited to a narrow radius around the stimulating electrode and pharmacology experiments further confirmed that ganglion cells were directly activated: spikes were not suppressed in the presence of CNQX, APV, and kynurenate, which block excitatory transmission in the retina (Fujimoto and Toyoda 1991; Stett et al. 2000). This is a much more local effect than can be achieved with larger electrodes: indirect spikes sensitive to synaptic blockers have been reported for 125-μm electrodes (Jensen et al. 2002; Ziv et al. 2002) and larger electrodes (Greenberg 1998; Shimazu et al. 1999). Our results from simultaneous stimulation using multiple electrodes further confirm that the current spread in the plane of the electrode array is small enough to allow for independent activation of cells using neighboring stimulation electrodes.

Thresholds increase with the distance between stimulating and recording electrode on the array (see Fig. 5*A*). The observed increases are similar to those of the cathodal stimulation map reported by Jensen et al. (2003): stimulating about 60 μm away from the center of the receptive field required 2–8 times more current to elicit a spike.

Stimulation at amplitudes significantly above threshold activates cells in a larger radius around the stimulation site (Fig. 5*B*). However, such high stimulus strengths are unlikely to be required during normal operation of a high-resolution implant. A large number of perceived gray levels may be achieved by varying the pulse frequency, thus eliciting spike trains of different rates in individual ganglion cells (Fig. 7*C*). Limiting stimulation strength to 2–3 times the threshold therefore can achieve a high spatial resolution without reducing the dynamic range of stimulation.

We conclude from our observations that retinal implants with small electrodes can achieve a high spatial resolution, because the low required currents activate single (or at most a few) ganglion cells.

CHRONAXIES AND SITE OF ACTIVATION. The use of pulses significantly longer than chronaxie contributes little to the evoked response, stipulating pulse durations smaller than chronaxie to insure that most of the applied charge contributes to evoking a response (Tehovnik 1996). Thus from the chronaxies measured in this study (~100–400 μs), we conclude that optimal pulse durations should not exceed this range.

TABLE 1. *Literature analysis*

				Pulse			Electrode		Threshold					
	Electrode	Species	Condition	Shape	Duration ms	Frequency Hz	Diameter μm	Area μm^2	Definition	Current μA	Current density nA/μm^2	Charge nC	Charge density mC/cm^2	Notes
* Doty & Grimm 1962	Bipolar	Cat		Monophasic	1	0.3	200	3.1E+04	Cortex	100	3.2	100	0.32	Data from Fig. 6 and Gekeler et al. 2004
Dawson & Radtke 1977	Monopolar	Cat		Monophasic	0.8	0.2	25	7.7E+04	Cortex	30	0.4	24	0.03	3 electrodes were joined together; surface area calculated from charge density
Humayun et al. 1994	Bipolar	Rabbit		Biphasic	0.075	1	200	1.3E+05	ERG	150	1.2	11	0.009	Spherical electrodes
Wyatt et al. 1994	Monopolar	Rabbit		Monophasic	0.1		25	4.9E+02		14	29	1.4	0.29	Data for Pt/Ir electrodes used
Rizzo et al. 1996	Array	Rabbit		Biphasic	0.05		40	1.6E+03	Cortex	180	113	9	0.56	Lowest threshold used
Humayun et al. 1996	Bi/monopolar	Human		Biphasic	1	0.5–2	200	1.3E+05	Percept	500	4	500	0.40	Median threshold of all probe 1 data used
* Rizzo et al. 1997	Bipolar	Rabbit		Monophasic	0.2	4–5	25	4.9E+02	50%	8	16.3	1.60	0.33	
	Monopolar				0.1		5	2.0E+01		0.5	25	0.05	0.25	Median cell body thresholds used
* Peixoto et al. 1998	Array	Rabbit		Biphasic	0.75		100	1.0E+04	Cortex	45	5	34	0.34	Stimulus consisted of 5–10 pulses, 100 μs each
Grumet et al. 1998	Array	Salamander		Biphasic	0.1		10	7.9E+01		4	51	0.4	0.51	Lowest typical threshold used
Greenberg 1998	Monopolar	Human		Biphasic	1		700	3.8E+05	Percept	1200	3.1	1200	0.31	Data from patient C.S. used
		Frog		Monophasic	0.52		400	1.3E+05	75%	125	1.0	65	0.05	
Humayun et al. 1999a	Array	Human	Large electrode	Biphasic	2	1–50	400	1.3E+05	Percept	200	1.6	400	0.32	Data for subject H.C. used
	Monopolar		Smaller electrode	Biphasic		1	125	1.2E+04		550	45	1100	8.97	Average over all probe 3 data used
Grumet 1999	Array	Rabbit		Biphasic	0.4		10	7.9E+01	50%	0.15	1.9	0.06	0.08	Axons stimulated; data from Table 3.4 used
Nadig 1999	Bipolar	Rabbit		Biphasic	0.1	0.5–10	550	2.4E+05	Cortex	238	1.0	24	0.01	Lowest threshold used
Weiland et al. 1999	Monopolar	Human	Subject 1	Biphasic	1	1	125	1.2E+04	Percept	100	8.2	100	0.82	
			Subject 2							600	49	600	4.89	
* Rizzo et al. 1999	Array	Rabbit	Monopolar		0.2	0.5–16	100	7.9E+03		75	9.6	15	0.19	Data from Gekeler et al. 2004 and Rizzo et al. 2003
			Bipolar		0.1					100	12.7	10	0.13	
Hesse et al. 2000	Array	Cat		Biphasic	0.4		100	1.0E+04	Cortex	50	5.0	20	0.20	
Walter & Heimann 2000	Array	Rabbit		Mono/biphasic	0.5	1	100	2.0E+04	Cortex	20	1.0	10	0.05	Stimulus consisted of 5–10 pulses, 100 μs each
Rizzo et al. 2000	Array	Human	Normal sight		2		400	1.3E+05	Percept	50	0.4	100	0.08	
					2		100	7.9E+03		12	1.5	24	0.31	
			RP patient		0.25		400	1.3E+05		1500	11.9	375	0.30	
					0.16		100	7.9E+03		60	7.6	10	0.12	
Grumet et al. 2000	Array	Rabbit		Biphasic	0.4	10	10	7.9E+01	50%	0.25	3.2	0.10	0.13	Axons stimulated; threshold data from Fig. 5
Schanze et al. 2002	Array	Cat	Fiber electrode	Biphasic	0.2		80	5.0E+03	Cortex	20	4.0	4	0.08	
			Film electrode				100	7.9E+03		40	5.1	8	0.10	
Wilms et al. 2003	Monopolar	Cat		Biphasic	0.2	5–7	25	8.5E+02	Cortex	11	13	2	0.26	
Laube et al. 2003	Bipolar	Pig		Biphasic	1	1	70	3.8E+03	Cortex	50	13.0	50	1.30	Stimulus was a train of 5 pulses, 200 μs each
Humayun et al. 2003	Array	Human		Biphasic	1		520	2.1E+05	Percept	350	1.6	350	0.16	Threshold: average of all subjects in Fig. 3
Jensen et al. 2003	Monopolar	Rabbit		Monophasic	0.1	4–5	2	1.6E+01	50%	0.5	31	0.05	0.31	
* Humayun 2003	Array	Human	Subject 1	Biphasic	1		520	2.1E+05	Percept	450	2.1	450	0.21	
			Subject 3							50	0.24	50	0.02	
Rizzo et al. 2003a,b	Array	Human	Normal sight	Biphasic	2	6–20	100	7.9E+03	Percept	12	1.5	24	0.31	Selected examples from Table 3 are shown
			RP patient 3		8		400	1.3E+05		441	3.5	3528	2.81	
			RP patient 5		4		400	1.3E+05		200	2	800	0.64	
Suzuki et al. 2004	Monopolar	Mouse	Short dur	Biphasic	0.12		125	1.2E+04	67%	500	41	60	0.49	
			Medium dur		0.5					240	20	120	0.98	Data from Figs. 3 and 4 used
			Long dur		1					180	15	180	1.47	
Johnson et al. 2004	Array	Rabbit	Large electrode	Biphasic	1		1800	2.5E+06	50%	756	0.30	756	0.03	Threshold was 50% of maximum population spike number; data from Fig. 5 used
			Smaller electrode				160	2.0E+04		15	0.75	15	0.07	
Kuras et al. 2004	Bipolar	Frog			0.05	0.5	40	1.3E+03	50%	12	9.6	1	0.05	Lowest threshold used
Jensen et al. 2005a	Monopolar	Rabbit		Monophasic	1	2	125	1.2E+04	50%	15	1.2	15	0.12	Data from Fig. 2 used
Jensen et al. 2005b	Monopolar	Rabbit		Monophasic	0.1	2–3	125	1.2E+04	50%	0.75	0.06	0.08	0.001	
Zehnder et al. 2005	Array	Human			1		360	1.0E+05	Percept	191	1.9	191	0.19	
This study	Array	Rat	Stim & rec same electrode	Biphasic	0.1	1–2	6.3	3.1E+01	90%	0.6	19.1	0.06	0.19	
					0.05		8.6	5.8E+01		0.9	16.1	0.05	0.08	
					0.05		12.7	1.3E+02		1.3	10.5	0.07	0.05	
		Monkey	Stim & rec separate		0.1		9	6.4E+01		1.5	23.6	0.15	0.24	

Data from 32 studies which reported thresholds for epiretinal simulation, and four representative examples from this study. The *Electrode* column lists needle-shaped probes as bi- or monopolar; *array* indicates a multi-electrode array in monopolar configuration unless otherwise noted. Multiple table entries were made if different parameters (species, electrodes, pulses) were reported, see *Condition* column. Threshold definition: percentage indicates the current at which that percent of trial pulses evoked a spike; *cortex* indicates evoked potential recordings in the visual cortex; *percept* indicates phosphene detection in humans. The *Notes* column lists additional information on the compilation of data. Asterisks mark studies for which a parameter was substituted from other publications by the same author or group. ERG, electroretinogram.

The measured values are similar to those reported in other studies (Crapper and Noell 1963; Greenberg 1998; Grumet et al. 2000; Jensen et al. 2005b) and can further be used to identify the neuronal element most likely excited by electrical stimulation. Our chronaxies match those reported for activation of axons (Grumet et al. 2000; Holsheimer et al. 2000; Nowak and Bullier 1998), because cell bodies and dendrites have chronaxies of 1–10 ms (Holsheimer et al. 2000; Ranck 1975). Because the initial axon segment near somas is more excitable than cell bodies (Greenberg et al. 1999; Nowak and Bullier

1998; Porter 1963; Schiefer and Grill 2002), the juxtasomal electrode used here likely activates this initial region on the axon and action potentials subsequently backpropagate a short distance to elicit the recorded somatic spike. Computational models suggest that excitation occurs near the junction of ganglion cell soma and axon or slightly more distal on the axon (Fohlmeister and Miller 1997; McIntyre and Grill 1999; Schiefer and Grill 2002).

It is difficult to experimentally rule out the activation of passing axons, in particular because tests designed to identify antidromic responses (Fuller and Schlag 1976) would not distinguish between initial axon segment excitation and more distant axon activation. Nevertheless, activation of passing axons is deemed less likely by the fact that ganglion cell axons have high thresholds away from their initial segment (Loeb et al. 1983). Because in retinal ganglion cells of most mammals (including human and rat) the axon remains unmyelinated within the retina, sodium channels are found uniformly throughout the unmyelinated region distant from the soma (Boiko et al. 2003). At the initial axon segment, however, the density of sodium channels is exceptionally high (Wollner and Catterall 1986), with clustering of the $Na_v1.6$ subunit in particular (Boiko et al. 2003). This difference in channel density between the initial and distant region can amount to an order of magnitude or more (Ritchie et al. 1976; S. R. Levinson, personal communication). Like the nodes of Ranvier in myelinated fibers (McIntyre and Grill 2000), the initial portion of unmyelinated axons constitutes the most likely site of electrical excitation, perhaps at the "thin segment" 10–40 μm from the cell body (Boiko et al. 2003; Fohlmeister and Miller 1997).

Comparative literature analysis

To discuss data from this study in the context of previous work, a comprehensive review of the published literature was composed. Table 1 summarizes 32 studies that have reported epiretinal stimulation thresholds. These studies span several orders of magnitude in electrode size and can thus be used to elucidate threshold trends. Several key parameters have been graphed in Fig. 11, along with best fit lines and correlation

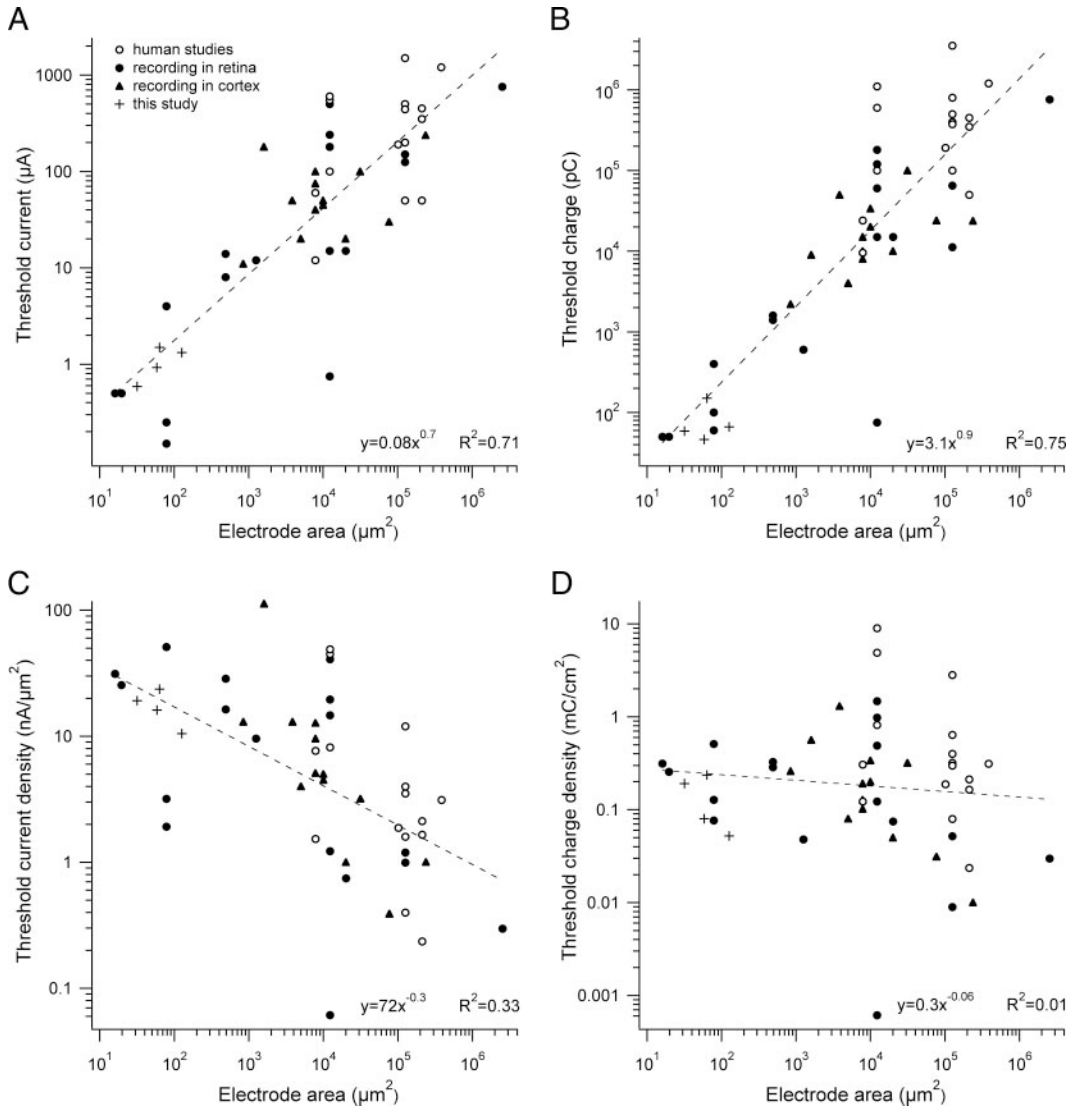

FIG. 11. Literature analysis. Data from Table 1 plotted for current, charge, current density, and charge density at threshold. Human studies are shown as open circles and representative examples from this study as crosses. Solid symbols indicate animal studies which either recorded neuronal responses in the retina (circles) or in the visual cortex (triangles). Dashed lines are best fits to the data, with the correlation coefficient R^2 and the fit line equation shown for each graph.

coefficients. To facilitate comparison of different electrode geometries across studies, threshold parameters were plotted against the geometric electrode surface area (see METHODS).

VARIABILITY. Several factors contribute to the relatively wide scatter of points in Fig. 11. Threshold was defined inconsistently from study to study, spanning the range of 50–90% probability of eliciting a spike, cortical recordings, and human percept reports. Furthermore, while the majority of studies used charge-balanced biphasic pulses, several reported monophasic stimulation (typically cathodal), leading to lower thresholds in some cases. Moreover, human studies (open symbols) usually involved degenerated retinas, whereas animal studies were typically performed on normal tissue. Finally, studies which measured retinal responses by monitoring cortical activity (triangles) may have overestimated spike thresholds in ganglion cells, because the concerted activity of many cells is typically required for a cortical response.

PARAMETER TRENDS. Both threshold current and charge (Fig. 11, *A* and *B*) decrease dramatically as electrode size is reduced. Correlation was highest for threshold charge, because it takes into account both current and pulse duration, which varied across studies. These trends confirm that smaller electrodes require several orders of magnitude lower currents to elicit responses. They also mirror the results found within this study over a much more narrow range of electrode sizes: current and charge thresholds were small for small stimulating electrodes and large for large electrodes (Fig. 10, *A* and *B*).

Current density also increases somewhat when electrode size is reduced (Fig. 11*C*), owing largely to the fact that studies using smaller electrodes also tended to apply shorter pulses (see Table 1). Such a trend is not seen in the plot of charge density thresholds (Fig. 11*D*). While the large variability does not permit an accurate fit to the data, there is no definitive change of charge density with electrode size, such as is seen for threshold charge over four to five orders of magnitude. In fact, charge density is virtually independent of electrode size for electrodes smaller than 10^4 μm^2 (disk diameter about <100 μm). This trend is in contrast to the increased charge densities observed for the smallest electrodes used in this study (see Fig. 10*D*), which is probably caused by an effect restricted to electrodes smaller than ~ 10 μm diam.

Representative data from this study (monkey and rat) have been included in Fig. 11 and fit well with the trends established by the published literature. Our data substantiate the main conclusion from this analysis: small electrodes require much less charge injection for threshold stimulation than larger electrodes, but the accompanying increase in charge density is almost negligible.

STIMULATION SAFETY. Because both charge and charge density must be considered when discussing stimulation safety (Merrill et al. 2005), Fig. 12 shows a plot of both parameters for the same set of studies. Two types of safety limit lines were included: the often used electrochemical limits for platinum (0.35 and 0.1 mC/cm^2) and iridium oxide electrodes (1 and 4 mC/cm^2), as well as the limits for neural injury from cortical stimulation data ($k = 1.7$ and 2.0; see METHODS). To show the spread of thresholds measured in this study, Fig. 12 includes data points for all cells stimulated using 0.05-ms pulses and electrodes with diameters between 6 and 25 μm (crosses).

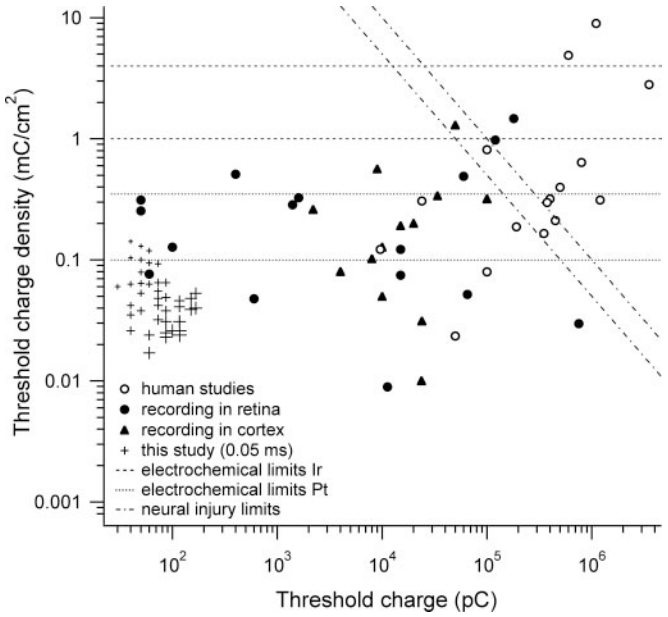

FIG. 12. Threshold charge density plotted against charge. Data from Table 1 were used, along with several safety limits, indicating the region of potentially safe and unsafe stimulation parameters. The plotted electrochemical limits are for platinum (0.1 and 0.35 mC/cm^2, dotted lines) and iridium oxide (1 and 4 mC/cm^2, dashed lines). Neural injury limits (dash-dotted lines) are from cortical stimulation data ($k = 1.7$ and 2. 0). Crosses are thresholds for 0.05-ms pulses from this study spanning all electrode diameters (6–25 μm; symbol size is proportional to electrode diameter).

Most human studies (and several animal studies) fall near or outside of the safe region formed by the neural injury limits, possibly because degenerated retina requires higher currents to produce phosphenes in humans. While most data points lie close to or above the electrochemical limits for platinum, it should be emphasized that the increase in effective surface area afforded by the electroplating process raises the true safety limits by at least an order of magnitude. Furthermore, electrodes made of materials such as iridium clearly have higher electrochemical limits (Beebe and Rose 1988; Merrill et al. 2005; Weiland et al. 2002) and may be used to substantially extend the region of safe stimulation.

Figure 12 validates our claim that the small electrodes used in this study can safely stimulate mammalian retina: except for the data collected using the smallest electrodes, most thresholds are well within all safety limits.

Outlook

The purpose of this study was to elucidate basic stimulation parameters to test whether a future generation of implants could incorporate a design using significantly smaller electrodes than are presently available. We used planar microelectrode arrays that closely resemble those currently in use for chronic human testing (Humayun et al. 2003) but contain much smaller electrodes at a much smaller electrode spacing. We suggest that future implants could directly activate ganglion cells instead of affecting large areas of retina by indirect stimulation, making possible a reasonable spatial resolution of artificial sight. One can envision high-resolution arrays containing thousands of stimulation sites with diameters around 10–20 μm and separation between electrodes of 20–60 μm.

While years away, results from this study suggest that there is no fundamental hindrance to the feasibility of such a device. Once implanted, the stimulus parameters can be adjusted to stimulate individual or small overlapping groups of ganglion cells, depending on the desired phosphene size. By using low currents, activation of axon bundles can be avoided. As a next step toward the development of such implants, further experiments using small electrodes with degenerated retina are warranted.

ACKNOWLEDGMENTS

We thank M. McMahon for constructive comments on the manuscript and vital feedback throughout this project.

GRANTS

This research was supported by the Salk Institute Pioneer Postdoctoral Fellowship, Second Sight Medical Products Inc., McKnight Foundation National Eye Institute Grants EY-13150 to (E. J. Chichilnisky) and EY-12893 (to Second Sight Medical Products), National Science Foundation Awards PHY-0245104 and PHY-0417175 (to A. M. Litke), Polish State Committee for Scientific Research, Project 3 T11E 011 27 (to W. Dabrowski), and NATO Collaborative Linkage Grant (to A. M. Litke and W. Dabrowski).

REFERENCES

Beebe X and Rose TL. Charge injection limits of activated iridium oxide electrodes with 0.2 ms pulses in bicarbonate buffered saline. *IEEE Trans Biomed Eng* 35: 494–495, 1988.

Benjamin A, Humayun M, Hickingbotham D, de Juan E, and van den Honert C. Characterization of retinal responses to electrical stimulation of retinal surface of rana catesbeiana (Abstract). *Invest Ophthalmol Vis Sci* 35: 1832, 1994.

Boiko T, Van Wart A, Caldwell JH, Levinson SR, Trimmer JS, and Matthews G. Functional specialization of the axon initial segment by isoform-specific sodium channel targeting. *J Neurosci* 23: 2306–2313, 2003.

Brummer SB, Robblee LS, and Hambrecht FT. Criteria for selecting electrodes for electrical stimulation: theoretical and practical considerations. *Ann NY Acad Sci* 405: 159–171, 1983.

Brummer SB and Turner MJ. Electrical stimulation with Pt electrodes: II-estimation of maximum surface redox (theoretical non-gassing) limits. *IEEE Trans Biomed Eng* 24: 440–443, 1977.

Cha K, Horch K, and Normann RA. Simulation of a phosphene-based visual field: visual acuity in a pixelized vision system. *Ann Biomed Eng* 20: 439–449, 1992a.

Cha K, Horch KW, and Normann RA. Mobility performance with a pixelized vision system. *Vision Res* 32: 1367–1372, 1992b.

Chichilnisky EJ and Baylor DA. Receptive-field microstructure of blue-yellow ganglion cells in primate retina. *Nat Neurosci* 2: 889–893, 1999.

Crapper DR and Noell WK. Retinal excitation and inhibition from direct electrical stimulation. *J Neurophysiol* 26: 924–947, 1963.

Dabrowski W, Grybos P, Hottowy P, Skoczen A, Swientek K, Grillo AA, Kachiguine S, Litke AM, and Sher A. Development of front-end ASICs for imaging neuronal activity in live tissue. *Nucl Instrum Methods Phys Res A* 541: 405–411, 2005.

Dawson WW and Radtke ND. The electrical stimulation of the retina by indwelling electrodes. *Invest Ophthalmol Vis Sci* 16: 249–252, 1977.

Devries SH and Baylor DA. Mosaic arrangement of ganglion cell receptive fields in rabbit retina. *J Neurophysiol* 78: 2048–2060, 1997.

Doty RW and Grimm FR. Cortical responses to local electrical stimulation of retina. *Exp Neurol* 5: 319–334, 1962.

Fohlmeister JF and Miller RF. Mechanisms by which cell geometry controls repetitive impulse firing in retinal ganglion cells. *J Neurophysiol* 78: 1948–1964, 1997.

Fujimoto M and Toyoda J. An analysis of inputs to ON-OFF amacrine cells in the carp retina with kynurenic acid. *Neuroreport* 2: 317–320, 1991.

Fuller JH and Schlag JD. Determination of antidromic excitation by the collision test: problems of interpretation. *Brain Res* 112: 283–298, 1976.

Gekeler F, Kobuch K, Schwahn HN, Stett A, Shinoda K, and Zrenner E. Subretinal electrical stimulation of the rabbit retina with acutely implanted electrode arrays. *Graefes Arch Clin Exp Ophthalmol* 242: 587–596, 2004.

Greenberg R. *Analysis of Electrical Stimulation of the Vertebrate Retina - Work Towards a Retinal Prosthesis* (dissertation). Baltimore MD, John Hopkins University, 1998.

Greenberg RJ, Velte TJ, Humayun MS, Scarlatis GN, and de Juan E. A computational model of electrical stimulation of the retinal ganglion cell. *IEEE Trans Biomed Eng* 46: 505–514, 1999.

Grumet AE. *Electric Stimulation Parameters for an Epi-Retinal* Prosthesis (dissertation). Department of Electrical Engineering and Computer Science, Cambridge, MA: Massachusetts Institute of Technology, 1999.

Grumet AE, Wyatt JL, and Rizzo JF. Multi-electrode recording and stimulation of the salamander retina in vitro. *Invest Ophthalmol Vis Sci* 39: S565, 1998.

Grumet AE, Wyatt JL Jr, and Rizzo JF. Multi-electrode stimulation and recording in the isolated retina. *J Neurosci Methods* 101: 31–42, 2000.

Heckenlively JR, Boughman J, and Friedman L. Diagnosis and classification of retinitis pigmentosa. In: *Retinitis Pigmentosa*, edited by Heckenlively JR. Philadelphia, PA: Lippincott, 1988, p. 21.

Hesse L, Schanze T, Wilms M, and Eger M. Implantation of retina stimulation electrodes and recording of electrical stimulation responses in the visual cortex of the cat. *Graefes Arch Clin Exp Ophthalmol* 238: 840–845, 2000.

Holsheimer J, Demeulemeester H, Nuttin B, and de Sutter P. Identification of the target neuronal elements in electrical deep brain stimulation. *Eur J Neurosci* 12: 4573–4577, 2000.

Humayun MS. Clinical trial results with a 16-electrode epiretinal implant in end-stage RP patients. In: *The First DOE International Symposium on Artificial Sight*, edited by Humayun MS and Greenbaum E. Fort Lauderdale, FL: Department of Energy, 2003.

Humayun MS, de Juan E Jr, Dagnelie G, Greenberg RJ, Propst RH, and Phillips DH. Visual perception elicited by electrical stimulation of retina in blind humans. *Arch Ophthalmol* 114: 40–46, 1996.

Humayun MS, de Juan E Jr, Weiland JD, Dagnelie G, Katona S, Greenberg R, and Suzuki S. Pattern electrical stimulation of the human retina. *Vision Res* 39: 2569–2576, 1999.

Humayun MS, Propst R, de Juan E Jr, McCormick K, and Hickingbotham D. Bipolar surface electrical stimulation of the vertebrate retina. *Arch Ophthalmol* 112: 110–116, 1994.

Humayun MS, Weiland JD, Fujii GY, Greenberg R, Williamson R, Little J, Mech B, Cimmarusti V, Van Boemel G, Dagnelie G, and de Juan E. Visual perception in a blind subject with a chronic microelectronic retinal prosthesis. *Vision Res* 43: 2573–2581, 2003.

Jensen RJ, Rizzo JF III, Ziv OR, Grumet A, and Wyatt J. Thresholds for activation of rabbit retinal ganglion cells with an ultrafine, extracellular microelectrode. *Invest Ophthalmol Vis Sci* 44: 3533–3543, 2003.

Jensen RJ, Ziv OR, and Rizzo JF. Stimulation of ganglion cells in rabbit retina with a microelectrode placed on the inner retinal surface. In: *Proceedings of the Rehabilitation Research and Development 3rd National Meeting*, Arlington, VA: Department of Veterans Affairs, 2002, p. 92.

Jensen RJ, Ziv OR, and Rizzo JF. Responses of rabbit retinal ganglion cells to electrical stimulation with an epiretinal electrode. *J Neural Engineer* 2: S16, 2005a.

Jensen RJ, Ziv OR, and Rizzo JF. Thresholds for activation of rabbit retinal ganglion cells with relatively large, extracellular microelectrodes. *Invest Ophthalmol Vis Sci* 46: 1486–1496, 2005b.

Johnson L, Perkins FK, O'Hearn T, Skeath P, Merritt C, Frieble J, Sadda S, Humayun M, and Scribner D. Electrical stimulation of isolated retina with microwire glass electrodes. *J Neurosci Methods* 137: 265–273, 2004.

Kim CS and Oh SM. Enzyme sensors by electrodeposition on platinized platinum electrodes. *Electrochim Acta* 41: 2433–2439, 1996.

Kim SY, Sadda S, Pearlman J, Humayun MS, de Juan E Jr, Melia BM, and Green WR. Morphometric analysis of the macula in eyes with disciform age-related macular degeneration. *Retina* 22: 471–477, 2002.

Klein R, Klein BE, Jensen SC, and Meuer SM. The five-year incidence and progression of age-related maculopathy: the Beaver Dam Eye Study. *Ophthalmology* 104: 7–21, 1997.

Kuras A, Baginskas A, and Batuleviciene V. Suprathreshold excitation of frog tectal neurons by short spike trains of single retinal ganglion cell. *Exp Brain Res* 159: 509–518, 2004.

Kuras A and Gutmaniene N. Multi-channel metallic electrode for threshold stimulation of frog's retina. *J Neurosci Methods* 75: 99–102, 1997.

Lapicque L. Recherches quantitatives sur l'excitation electrique des nerfs traites comme un polarization. *J Physiol Paris* 9: 620–635, 1907.

Laube T, Schanze T, Brockmann C, Bolle I, Stieglitz T, and Bornfeld N. Chronically implanted epidural electrodes in Gottinger minipigs allow function tests of epiretinal implants. *Graefes Arch Clin Exp Ophthalmol* 241: 1013–1019, 2003.

Litke AM. The retinal readout system: an application of microstrip detector technology to neurobiology. *Nucl Instrum Methods Phys Res A* 418: 203–209, 1998.

Litke AM. The retinal readout system: a status report. *Nucl Instrum Methods Phys Res A* 435: 242–249, 1999.

Litke AM, Chichilnisky EJ, Dabrowski W, Grillo AA, Grybos P, Kachiguine S, Rahman M, and Taylor G. Large-scale imaging of retinal output activity. *Nucl Instrum Methods Phys Res A* 501: 298–307, 2003.

Loeb GE, White MW, and Jenkins WM. Biophysical considerations in electrical stimulation of the auditory nervous system. *Ann NY Acad Sci* 405: 123–136, 1983.

Mathieson K, Kachiguine S, Adams C, Cunningham W, Gunning D, O'Shea V, Smith KM, Chichilnisky EJ, Litke AM, Sher A, and Rahman M. Large-area microelectrode arrays for recording of neural signals. *IEEE Trans Nuc Sci* 51: 2027–2031, 2004.

McCreery DB, Agnew WF, Yuen TG, and Bullara L. Charge density and charge per phase as cofactors in neural injury induced by electrical stimulation. *IEEE Trans Biomed Eng* 37: 996–1001, 1990.

McCreery DB, Bullara LA, and Agnew WF. Neuronal activity evoked by chronically implanted intracortical microelectrodes. *Exp Neurol* 92: 147–161, 1986.

McIntyre CC and Grill WM. Excitation of central nervous system neurons by nonuniform electric fields. *Biophys J* 76: 878–888, 1999.

McIntyre CC and Grill WM. Selective microstimulation of central nervous system neurons. *Ann Biomed Eng* 28: 219–233, 2000.

Meister M, Pine J, and Baylor DA. Multi-neuronal signals from the retina: acquisition and analysis. *J Neurosci Methods* 51: 95–106, 1994.

Merrill DR, Bikson M, and Jefferys JG. Electrical stimulation of excitable tissue: design of efficacious and safe protocols. *J Neurosci Methods* 141: 171–198, 2005.

Nadig MN. Development of a silicon retinal implant: cortical evoked potentials following focal stimulation of the rabbit retina with light and electricity. *Clin Neurophysiol* 110: 1545–1553, 1999.

Narayanan MV, Rizzo JF, Edell DJ, and Wyatt J. Development of a silicon retinal implant: cortical evoked potentials following focal stimulation of the rabbit retina with light and electricity (Abstract). *Invest Ophthalmol Vis Sci* 35: 1380, 1994.

Nowak LG and Bullier J. Axons, but not cell bodies, are activated by electrical stimulation in cortical gray matter. I. Evidence from chronaxie measurements. *Exp Brain Res* 118: 477–488, 1998.

Palanker DV, Huie P, Vankov AB, Freyvert Y, Fishman H, Marmor MF, and Blumenkranz MS. Attracting retinal cells to electrodes for high-resolution stimulation. In: *Proceedings of SPIE, Ophthalmic Technologies XIV*, edited by Manns F, Soderberg PG, and Ho A. Bellingham, WA: The International Society for Optical Engineering, 2004, vol. 5314, p. 306–314.

Peixoto N, Strassburger S, Hornig R, Walter P, Szurman P, and Eckmiller R. Evaluation of implanted epiretinal microcontacts in the mammalian retina (Abstract). *Invest Ophthalmol Vis Sci* 39: S902, 1998.

Plonsey R and Barr RC. *Bioelectricity. A Quantitative Approach.* New York: Plenum Press, 1988, p. 281–286.

Pollen DA. Responses of single neurons to electrical stimulation of the surface of the visual cortex. *Brain Behav Evol* 14: 67–86, 1977.

Porter R. Focal stimulation of hypoglossal neurones in the cat. *J Physiol* 169: 630–640, 1963.

Ranck JB. Which elements are excited in electrical stimulation of mammalian central nervous system: a review. *Brain Res* 98: 417–440, 1975.

Ritchie JM, Rogart RB, and Strichartz GR. A new method for labelling saxitoxin and its binding to non-myelinated fibres of the rabbit vagus, lobster walking leg, and garfish olfactory nerves. *J Physiol* 261: 477–494, 1976.

Rizzo JF, Grumet AE, Edell DJ, Wyatt JL, and Jensen RJ. Single-unit recording following extracellular stimulation of retinal ganglion cell axons in rabbits (Abstract). *Invest Ophthalmol Vis Sci* 38: S40, 1997.

Rizzo JF, Loewenstein J, and Wyatt JL. Development of an epiretinal electronic visual prosthesis: the Harvard Medical School–Massachusetts Institute of Technology Research Program. In: *Retinal Degenerative Diseases and Experimental Therapy*, edited by Hollyfield JG, Anderson RE, and LaVail MM. New York: Kluwer Academic/Plenum Publishers, 1999, p. 463.

Rizzo JF, Miller S, Denison T, Herndon T, and Wyatt JL. Electrically-evoked cortical potentials from stimulation of rabbit retina with a microfabricated electrode array (Abstract). *Invest Ophthalmol Vis Sci* 37: S707, 1996.

Rizzo JF and Wyatt J. Prospects for a visual prosthesis. *Neuroscientist* 3: 251–262, 1997.

Rizzo JF, Wyatt J, Loewenstein J, and Kelly S. Acute intraocular retinal stimulation in normal and blind humans (Abstract). *Invest Ophthalmol Vis Sci* 41: S102, 2000.

Rizzo JF, Wyatt J, Loewenstein J, Kelly S, and Shire D. Methods and perceptual thresholds for short-term electrical stimulation of human retina with microelectrode arrays. *Invest Ophthalmol Vis Sci* 44: 5355–5361, 2003a.

Rizzo JF, Wyatt J, Loewenstein J, Kelly S, and Shire D. Perceptual efficacy of electrical stimulation of human retina with a microelectrode array during short-term surgical trials. *Invest Ophthalmol Vis Sci* 44: 5362–5369, 2003b.

Rose TL and Robblee LS. Electrical stimulation with Pt electrodes. VIII. Electrochemically safe charge injection limits with 0.2 ms pulses. *IEEE Trans Biomed Eng* 37: 1118–1120, 1990.

Santos A, Humayun MS, de Juan E Jr, Greenburg RJ, Marsh MJ, Klock IB, and Milam AH. Preservation of the inner retina in retinitis pigmentosa. A morphometric analysis. *Arch Ophthalmol* 115: 511–515, 1997.

Schanze T, Wilms M, Eger M, Hesse L, and Eckhorn R. Activation zones in cat visual cortex evoked by electrical retina stimulation. *Graefes Arch Clin Exp Ophthalmol* 240: 947–954, 2002.

Schiefer MA and Grill WM. Excitation sites during epiretinal electrical stimulation. *33rd Annual Neural Prosthesis Workshop, NIH, Bethesda, MD, October* 2002.

Sekirnjak C, Hottowy P, Sher A, Dabrowski W, Litke AM, and Chichilnisky EJ. Electrical stimulation of mammalian retinal ganglion cells using dense arrays of small-diameter electrodes. In: *Artificial Sight; Springer Series Biological and Medical Physics/Biomedical Engineering*, edited by Humayun MS, Weiland JD, Chader G, and Greenbaum E. Fort Lauderdale, FL: Springer Verlag. In press.

Shannon RV. A model of safe levels for electrical stimulation. *IEEE Trans Biomed Eng* 39: 424–426, 1992.

Shimazu K, Miyake Y, and Watanabe S. Retinal ganglion cell response properties in the transcorneal electrically evoked response of the visual system. *Vision Res* 39: 2251–2260, 1999.

Stett A, Barth W, Weiss S, Haemmerle H, and Zrenner E. Electrical multisite stimulation of the isolated chicken retina. *Vision Res* 40: 1785–1795, 2000.

Stone JL, Barlow WE, Humayun MS, de Juan EJ, and Milam AH. Morphometric analysis of macular photoreceptors and ganglion cells in retinas with retinitis pigmentosa. *Arch Ophthalmol* 110: 1634–1639, 1992.

Suzuki S, Humayun MS, Weiland JD, Chen SJ, Margalit E, Piyathaisere DV, and de Juan E Jr. Comparison of electrical stimulation thresholds in normal and retinal degenerated mouse retina. *Jpn J Ophthalmol* 48: 345–349, 2004.

Tehovnik EJ. Electrical stimulation of neural tissue to evoke behavioral responses. *J Neurosci Methods* 65: 1–17, 1996.

Troy JB and Robson JG. Steady discharges of X and Y retinal ganglion cells of cat under photopic illuminance. *Vis Neurosci* 9: 535–553, 1992.

Wagenaar DA and Potter SM. Real-time multi-channel stimulus artifact suppression by local curve fitting. *J Neurosci Methods* 120: 113–120, 2002.

Walter P and Heimann K. Evoked cortical potentials after electrical stimulation of the inner retina in rabbits. *Graefes Arch Clin Exp Ophthalmol* 238: 315–318, 2000.

Weiland JD, Anderson DJ, and Humayun MS. In vitro electrical properties for iridium oxide versus titanium nitride stimulating electrodes. *IEEE Trans Biomed Eng* 49: 1574–1579, 2002.

Weiland JD, Humayun MS, Dagnelie G, de Juan E Jr, Greenberg RJ, and Iliff NT. Understanding the origin of visual percepts elicited by electrical stimulation of the human retina. *Graefes Arch Clin Exp Ophthalmol* 237: 1007–1013, 1999.

Wilms M, Eger M, Schanze T, and Eckhorn R. Visual resolution with epi-retinal electrical stimulation estimated from activation profiles in cat visual cortex. *Vis Neurosci* 20: 543–555, 2003.

Wollner DA and Catterall WA. Localization of sodium channels in axon hillocks and initial segments of retinal ganglion cells. *Proc Natl Acad Sci USA* 83: 8424–8428, 1986.

Wyatt J, Rizzo JF, Grumet A, Edell DJ, and Jensen RJ. Development of a silicon retinal implant: epiretinal stimulation of retinal ganglion cells in the rabbit (Abstract). *Invest Ophthalmol Vis Sci* 35: 1380, 1994.

Zehnder T, Hornig R, Velikay-Parel M, Laube T, Bornfeld N, Feucht M, and Richard G. The IIP retinal implant. In: *Artificial Sight; Springer Series Biological and Medical Physics/Biomedical Engineering*, edited by Humayun MS, Weiland JD, Chader G, and Greenbaum E. New York: Springer Verlag. In press.

Ziv OR, Jensen RJ, and Rizzo JF. In vitro activation of ganglion cells in rabbit retina: effects of glutamate receptor agents. *Invest Ophthalmol Vis Sci* 43: E-abstract 4474, 2002.

Zrenner E, Stett A, Weiss S, Aramant RB, Guenther E, Kohler K, Miliczek KD, Seiler MJ, and Haemmerle H. Can subretinal microphotodiodes successfully replace degenerated photoreceptors? *Vision Res* 39: 2555–2567, 1999.